AN ABSTRACT OF THE THESIS OF

DONALD ASHLEY MILLER (Name) for the MASTER OF SCIENCE (Degree)

in CHEMISTRY (Major) presented on November 20, 1973 (Date)

Title: CHEMICAL COMPOSITION OF LAYERED GABBROS AND MINERAL SEPARATES FROM THE RED SEA AREA

Abstract approved: Redacted for Privacy
Roman A. Schmitt

Seventy samples that include basalts, gabbros, xenoliths, mineral separates, and standard rocks were analyzed by instrumental and radiochemical neutron activation analysis for about 25 elements. These samples, except for 12 basalts from the Picture Gorge region of Oregon, U.S.A. and the standard rocks, were collected from the southwest Saudi Arabian (SA) region of the Red Sea area.

Two SA gabbro series one a Miocene (Jabal at Turf, JT) and the other Precambrian (Jabal Shayi, JS) show similar bulk, minor and trace element abundances; also, the REE patterns are very similar and all show a positive Eu anomaly. The associated chillzone material for the Miocene gabbros has a REE pattern that is different from the gabbros. The REE abundance for the gabbros may be derived by fractional crystallization of the chillzone material. One of the gabbro samples is a unique sample in that it has a very high (~70%)

plagioclase content and shows a distinct REE pattern similar to that observed in the plagioclase separates analyzed. The JT and JS gabbros show no significant difference in composition due to the height variation.

Xenoliths, picked from coastal plain basalts, are of two distinct rock and mineral types. The xenoliths from JT basalts are of the lherzolite group which is mainly olivine with some pyroxenes present. The JT xenoliths show low Al, Ca and Na contents and therefore have a low plagioclase content. These samples have REE patterns that resemble those of plagioclase but much lower in total REE content. The Jabal Haylah (JH) xenoliths are from the eclogite (websterite) series of rocks. These rocks are mainly clinopyroxene with some orthopyroxene. The chondritic normalized REE patterns in the JH xenoliths are dome shaped with the La and Lu at approximately equal values; Sm and Eu are enriched by a factor of about two to three times relative to La. Both sets of xenoliths show extremely large Cr_2O_3 contents of ~1%. The bulk composition of these two series of xenoliths fall into the major element fields as described by Kuno (1969).

Mineral partition coefficients for plagioclase were determined relative to the gabbroic matrix. No differences were observed in the REE patterns in plagioclase separates from both the JT and JS layered gabbros.

The Sirat Plateau basalts analyzed in this work were similar in all respects to those analyzed by D. Coles (1972).

REE patterns observed in JS and JT layered gabbros are similar to those observed in two unique Apollo 15 basaltic rake samples, 15388 and 15643.

Chemical Composition of Layered Gabbros and Mineral Separates from the Red Sea Area

by

Donald Ashley Miller

A THESIS

submitted to

Oregon State University

in partial fulfillment of
the requirements for the
degree of

Master of Science

June 1974

APPROVED:

Redacted for Privacy

Professor of Chemistry

in charge of major

Redacted for Privacy

Head of Department of Chemistry

Redacted for Privacy

Dean of Graduate School

Date thesis is presented November 20, 1973

Typed by Clover Redfern for Donald Ashley Miller

ACKNOWLEDGMENTS

I am most grateful to my wife, Diana, for her patience and help both in putting up with the hours needed to produce this thesis and in typing the rough draft.

I would like to thank the author of the previous thesis on this subject, Mr. David G. Coles, for his work and leads. This paper was undertaken with the backing and stimulus of my major professor, Dr. Roman A. Schmitt. Dr. Schmitt not only provided the financial assistance through a research assistantship, but also valuable knowledge and encouragement.

My appreciation is also extended to Dr. Robert G. Coleman of the U.S. Geological Survey, Menlo Park, California, for sample classification, sample preparation and location information. The initial source of the samples was the Directorate General of Mineral Resources, Ministry of Petroleum and Mineral Resources, Saudi Arabia.

I would also like to thank Dr. Gordon Goles of the University of Oregon, Center for Volcanology, Eugene, Oregon, for sample collection and classification of the Picture Gorge samples that were analyzed at his request.

This work would not have been accomplished without the help and knowledge of Dr. J.C. Laul and Mr. David B. Curtis. These two

men were a valuable and available storehouse of geochemical knowledge.

I would also like to thank T. V. Anderson and his crew at the O.S.U. TRIGA Reactor for the activations. A. G. Johnson and his health physics staff were helpful during the experimental phases of this work.

Dr. William V. Boynton's programming of the Wang 500 calculator, which was used to process the data, is greatly appreciated. Dr. Boynton also helped in the radiochemical scheme for the determination of the REE.

Finally, I would like to thank the members of my committee, Dr. Schmitt and Dr. Julius Dasch for proof reading the manuscript and making comments which helped to improve considerably the quality of this thesis.

TABLE OF CONTENTS

LIST OF FIGURES

LIST OF TABLES

CHEMICAL COMPOSITION OF LAYERED GABBROS AND MINERAL SEPARATES FROM THE RED SEA AREA

I. INTRODUCTION

The Red Sea area has recently become interesting because of the possibility that it is an active site of tectonic (sea-floor spreading) movement. This would involve rifting and magmatic activity of the continent. This study is a continuation of a project that involves the chemical and geological make up of the Saudi Arabian portion of the Red Sea area. The determination of the chemical composition of various rock samples that represents the geological formations are of interest. In this particular part of the overall study gabbros and xenoliths are being studied along with some selected mineral separates. This may lead to some knowledge of how the region was formed.

Gabbros and Chillzone Rocks

The principle physicochemical factor in the evolution of various rocks from liquid magmas is a decrease in temperature, which causes crystallization. Crystal settling and removal process is called fractional crystallization (Goldschmidt, 1958). A process also to be considered is the effect of the various concentrations of the volatile substances present, such as CO_2, H_2O, F^-, Cl^-, etc. The volatile

elements have the effect of altering the reaction sequence of the magma crystallization. Chemical fractionation results in rocks that can be classified as gabbro-picrites, gabbros, etc. Solidification of the magma without extensive chemical fractionation gives the common olivine gabbros, ferrogabbros, etc.

The gabbros in this study exhibit fractional crystallization but most resemble the olivine gabbro series. Olivine gabbros have primary minerals of plagioclase, olivine and maybe some orthopyroxenes, iron oxides and apatite in small amounts. The ferrogabbros on the other hand have primary minerals or plagioclase, clinopyroxenes, olivine, ilmenite and magnetite with some quartz and apatite. The samples in this study consisted mainly of plagioclase, clinopyroxenes and olivine, therefore, these could be called olivine gabbros. The gabbros from the Skaergaard Layered Series show a sequence change of olivine gabbros passing into ferrogabbros as the layers go lower in the series (Hamilton, 1959).

Another aspect of gabbros is that they consist mainly of plagioclase and pyroxenes as the major minerals with these pure minerals as the extremes. At one end are the anorthosites, almost entirely composed of feldspars, and at the other end the plagioclase diminishes and there are rocks that approach the pyroxenites. The gabbroic magmas are characterized by relatively simple anions of the orthosilicate or metasilicates chain or ring types. This allows for a

variety of minerals to form in the crystallization. The gabbros therefore are composed of settled crystals and trapped interstitial magma to give their complexity of composition.

The overall character of the rare earth elements (REE) pattern in the original magma may be maintained intact in the magma during the differentiation. Since the upper layers of the series should be the last to crystallize and the REE tend to concentrate in the residual liquid, it seems reasonable that the upper layers are also enriched in the REE as compared to the lower, first crystallized layers. Again due to the concentration of the REE in the residual magma, any crystals that are formed are expected to have lower REE concentrations than the trapped interstitial liquids.

In trying to determine the sequence of fractionization the ratios of Na_2O:CaO and FeO:MgO can be used to approximate the degree of crystallization. These ratios increase as the sequence progresses. This could be helpful in determining if the layers are formed as suggested.

The associated chillzone rock is thought to have the composition of the original magma or part of the original magma. This magma cooled quickly without differentiation when it came into contact with the surrounding country rock. The chillzone rock is usually a fine grained olivine gabbro that may be similar to the alkali olivine basalts. In the samples analyzed for this study the Jabal at Turf (JT) chillzone

rock is from a well defined basal contact with the layers, while the Jabal Shayi (JS) chillzone rock is not so definite. The Jabal Shayi chillzone may be other magma that has upwelled by convection currents which could result in remelts instead of the original chillzone material.

The REE content and pattern of the chillzone may be similar to the other layers of the gabbroic sequence, but does not have to be. There should be no Eu anomalies present in the chillzone curve because there has been no depletion or enrichment of Eu due to the rapid crystallization.

Xenoliths

Exotic mafic and ultramafic inclusions called xenoliths found in basaltic rocks may be considered as representatives of cores from drillings performed by nature. These inclusions may or may not represent unique samples of the upper mantle and lower crust. Peridotites are the most common xenoliths and are found with pyroxenites, gabbros, and granulites. Eclogite is the other type of inclusion found and are associated with the peridotite inclusions only in limited numbers. The two xenolith types mainly differ in being derived from different pressure-temperature or mineral stability regions. The inclusions are everywhere confined to alkali basaltic rocks.

Peridotites may be either: 1) fragments of mantle from which basalts are produced, 2) residual solid material that remains after partial melting of the mantle material, or 3) crystal cumulates in basaltic magmas. Peridotites include dunites, lherzolite, wehrlites, harzburgite, etc. The lherzolites are uniform in mineral composition with olivine constituting up to approximately 60% of the rock. Also included are orthopyroxene, clinopyroxene, and chromium spinels. The inclusion of chromium spinels is common and will raise the Cr content considerably. The bulk chemical composition may also vary greatly.

Eclogite is defined as Mg rich garnets and Al rich pyroxenes (Kuno, 1969). Intermediate between the extreme types are rocks of the wehrlite series, which includes dunite with minor clinopyroxene. Lherzolite, wehrlite, and eclogite series may blend into each other during the scheme of crystallization.

The $MgO/\Sigma FeO$ is a good measure of the stage of fractional crystallization of magmas and the degree of partial melting. As the $MgO/\Sigma FeO$ content decreases in lherzolite, the Al_2O_3, ΣFeO, CaO, $Na_2O + K_2O$, TiO_2, and MnO contents increase and the MgO content decrease. At the same time the eclogite series experiences an increase in Al_2O_3, ΣFeO, $Na_2O + K_2O$, TiO_2 and MnO contents, while SiO_2, MgO, CaO, and Cr_2O_3 decrease (Kuno, 1969). With only this slight difference in CaO content to divide the group more

information is needed. The actual method of separation of lherzolite from eclogite will be shown later on in the discussion.

Xenoliths are difficult to classify because not everyone agrees on the labels or system of classification. I have tried to use one system and to check on its agreement. Harris et al. (1967) uses similar nomenclature as used by Kuno (1969), but the definitions of the terms due to the chemistry is reversed. Since I understood the discussion by Kuno, and my results showed good agreement with both chemical studies I will be using the definition by Kuno in this paper.

Mineral Partition Coefficients

A partition coefficient is defined as the content of an element in a mineral divided by the content of the same element in either the whole rock matrix or the residual liquid (Schnetzler and Philpotts, 1968). Trace elements are more sensitive indicators of differentiation processes in magmas because their partition coefficients are smaller and much more regular than the major elements. The partition coefficients are affected to a greater extent by the actual concentration of the element in the system, by changes in the composition of the crystallizing phases, and by saturation of the melt with any particular component. The partition coefficients are also affected by the pressure and temperature of the system at the time of crystallization (Philpotts and Schnetzler, 1970).

The best criteria of equilibrium which takes place during igneous melting is the uniformity of the partition coefficient pattern for each particular mineral (Schnetzler and Philpotts, 1970; Nagasawa et al., 1969). Regularity is commonly seen in the minerals, but occasionally deviations occur. The measured partition coefficients will only approximate the actual coefficients due to the problem of rim crystallization. This is due to the fact that the outer layer of a crystal is the only part that is in equilibrium with the residual melt or the surrounding rock. The interior of the rock sample may represent previous solid-liquid equilibrium states. Additional problems of diffusion have also been found but these are not as important as the rim problem. The partition coefficients approach a limiting value, called distribution constants, as the concentration of the element in the system decreases (Philpotts and Schnetzler, 1970; Paster et al., 1973). The difference from one system to the next of the trace element concentration may be due to the loss of volatile material during the solidification and cooling of the magma. This loss of volatile material is not very large in the complete sequence.

A unique chemical group for the study of partition coefficients is the REE. The REE variations during differentiations are due to partial fusion, equilibrium crystallization, fractional crystallization, and zone melting. The REE are concentrated differently in each of the mineral phases. Plagioclase is noted for its affinity for the light

REE and notably for its positive Eu anomaly. Also in the pyroxene minerals, Ca has a strong influence on the acceptance of the REE into the crystals. It is not exactly Ca but the size of the cation hole in the Ca minerals that are favorable for accommodation of REE. The main differences in the REE patterns between the various groups are due to the high pressure phase equilibria and the extent of partial fusion involved. There are also other elements that can be used such as Fe, Co, Sr, Sc, Ta, Zr, Hf, Th, and the alkali metals (Philpotts and Schnetzler, 1970), but these are not as consistent in their patterns or variations as are the REE.

Purpose

This work was a continuation of the geochemical study being done on the Saudi Arabian area of the Red Sea. This study was done in collaboration with Dr. Robert Coleman of the USGS (United States Geological Survey) Team of Menlo Park, California, U.S.A. The large volume of rock samples and mineral separates obtained from Dr. Coleman were divided into two groups; basalt samples and the gabbro-mineral separates. The first suite of basalt samples were analyzed by David Coles (1972) and I have done the second suite which contains layered gabbros, chillzone gabbros, xenoliths and the associated mineral-separates.

These samples were analyzed for the bulk, minor and trace

elements in order to determine the nature of the magmatic activity of the Red Sea area. This area is one of suggested recent continental break-up or rift and subsequent continental drift (Brown, 1973; Coleman, 1972; Coleman et al., 1973; Lowel et al., 1972; Shilling, 1971). With activity of this type it is common to find many varieties of rocks, including gabbroic intrusions, that are from various time periods located in a small area. This data may be compared with previous information obtained for gabbroic intrusions (Haskins et al., 1968; Paster et al., 1973; Kay and Senechal, 1973; Jensen, 1973; Schnetzler and Philpotts, 1970). Study of mineral separates may lead to some interesting information about the cooling history of the magmas and chillzone material.

Xenoliths are always of interest since they may give some knowledge about the chemical composition and possible fractionation history of mantle material. The xenoliths analyzed in this work seem to be very similar in many ways to the two groups shown by Harris et al. (1967), and Kuno (1969).

The 12 Picture Gorge basalts were analyzed at the request of Dr. Gordon G. Goles in order to determine their REE patterns as a comparison with the previous work of Osawa and Goles (1972).

Saudi Arabian Igneous Series Sample Description

Among the 70 samples analyzed in this work are ten analytical standard basalts and 45 whole rocks and mineral separates collected by Dr. R.G. Coleman of the USGS (United States Geological Survey) in a 1971 expedition to Saudi Arabia. The location of the sampling area is between 41°30' and 43°30' latitude and 16°30' and 19°00' longitude (see Figure 1).

Ten additional samples were obtained from Dr. G. Goles of the University of Oregon from the Picture Gorge area of Central Oregon, Oregon, U.S.A.

Samples SAB 486-492, SAB 215: These samples are layered gabbros from the Jabal at Turf complex of the MRZ (marginal rift zone), the age of which is 23 million years (Coleman, 1972). They are located within a narrow rift zone that marks the contact between the coastal plain sedimentary rocks and the Precambrian basement. They represent a sequential plagioclase-olivine-pyroxene set ranging from 0' to 5600' from the basal contact. The layered gabbros represent intruded basaltic magmas which were buried under the original surface rock. These are thought to have undergone considerable fractionation and differentiation to form coarse grained rocks with possible layers of minerals that have rhythmically crystallized and settled out during the fractionation process.

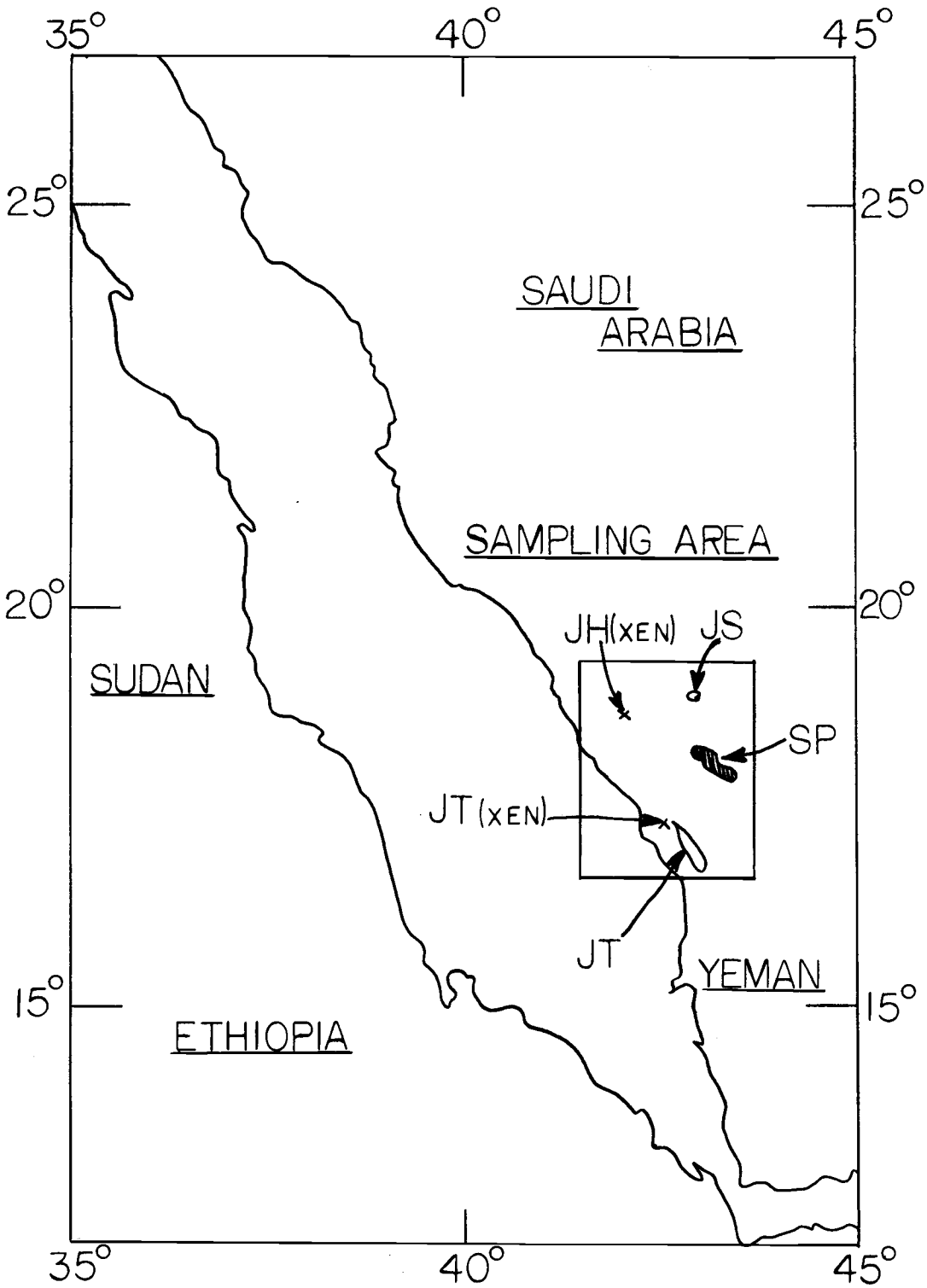

Figure 1. Map of Red Sea Area showing sampling locations.

SAB 215 is the associated chillzone for this series of layered gabbros. A chillzone is a contact zone between a hot magma and the country rock. Rocks of the chillzone are thought to very closely represent the original melt. This melt presumably cooled very quickly and allows no differentiation or crystal fractionation. This sample is definitely from the side of the exposed magma chamber where the chillzone area is located.

The classic example of an intrusive layered gabbro is the Skaergaard Intrusion in Eastern Greenland (Haskin and Haskin, 1967). The differentiation process of the Skaergaard Intrusion is further discussed in detail by Paster et al. (1973).

Samples SAB 476-485: All of these samples except SAB 483 and SAB 485 are layered gabbros from Jabal Shayi, with an age in the late pre-Cambrian. This group of samples is a sequential plagioclase-olivine-pyroxene set ranging from 0' to 6948' from the basal contact. This series of gabbros is very similar to the Jabal at Turf complex but are much older and some distance (~190 km) apart. SAB 483 and SAB 485 are considered to be the associated chillzone material for this set of layered gabbros. These particular samples may not be pure chillzone samples. This series of gabbros may be either a single flow or multiple flows which could have destroyed the previous chillzone areas.

Samples SAB 793-794: These samples are believed to be mantle

peridotite xenoliths from the Jabal at Turf complex. These two samples are two fragments from basalt sample SAB 217 (Coles, 1972) and are thought to be very similar to each other.

A xenolith is believed to be a part of the upper mantle or the original cognate material, that is carried along with the original melt (Wilkinson, 1967). Analysis of these samples may help us to understand either what the mantle is composed of or if we have premelt material of earlier years. These xenolith samples will in no way represent the melt that brought them to the surface as they were presumably always solidified when the melt was moving towards the surface.

Ultramafic xenoliths are common among alkali basalts and are either dunites or pyroxene-bearing peridotites. All of the xenoliths in the groups analyzed for this study are from the pyroxene-bearing type.

Samples SAB 795-797: These samples are thought to be mantle websterite xenoliths from the Jabal Haylah area of the Coastal Plain Complex. These samples are associated with the basalt sample SAB 253 (SAB 795) (Coles, 1972) and two are from the same larger sample which I did not analyze. As each xenolith is completely independent from all others this will allow me to obtain some information on the compositional variations of the upper mantle through which the magmas flowed before their emplacement.

Samples SAB 0794 and SAB C793: These two samples are orthopyroxene and clinopyroxene separates from the peridotite xenoliths SAB 793 and SAB 794. These xenoliths are pyroxene-bearing peridotites. Dr. Coleman separated some pyroxene minerals before crushing the remainder of the sample for analysis. Analysis of these samples will give us some insight into the partition coefficients of trace elements.

Sample SAB C797: This sample is a clinopyroxene mineral separate from a websterite xenolith from the Coastal Plain area. These crystals were removed from part of the xenolith by Dr. Coleman. The Coastal Plain basalts are alkali olivine basalts which cover large areas of the plains.

Sample SAB C246: This is a clinopyroxene mineral separate from the Sirat Plateau basalt feeder system. This is the only pyroxene separate from the actual basalt itself. The Sirat Plateau basalt feeders are thought to be part of extinct volcanos that fed the large basalt flows.

Samples CP-53 and CP-AHR: These two samples are clinopyroxene separates from alkali olivine basalt flows on Nunivak Island, Alaska, U.S.A. These samples are being analyzed to compare clinopyroxenes in two flows. These samples were obtained from Dr. Coleman as a comparison with the Saudi Arabian pyroxenes.

Sample CP-NId: This sample, obtained from Dr. Coleman, is a

chromium clinopyroxene from New Idria, California, U.S.A. This sample is listed as an alpine ultramafic pyroxenite. This sample was another comparison type of pyroxene.

Sample CR-SR: This sample is a clinopyroxene separate obtained from the Siletz River area of Oregon, U.S.A. This sample is from an alkali basalt. No further information was obtained about this sample.

Samples SAB P486-P492: These samples are plagioclase separates from the Jabal at Turf layered gabbros. Analysis of these samples will yield partition coefficient data for trace elements such as the REE in the plagioclases of the layered gabbros.

Samples SAB P478-P482 and SAB P484: This is a set of plagioclase separates from the Jabal Shayi layered gabbros of the Coastal Plain area. The objectives of interest in this group are similar to those indicated for the other plagioclase series.

Samples PG 6A & 6B, PG 7A & 7B, PG 9A & 9B, PG 12A & 12B, PG 16A & 16B: These samples are from the Picture Gorge area, Oregon, U.S.A. and were obtained from Dr. Gordon G. Goles, University of Oregon. The samples are all layered basalts collected by Goles and his associates. The samples labeled A and B are splits from the original sample collected.

PG 6 is a porphyrytic basalt with moderately-fine-grained ground mass. This sample contains two defined stages of crystals:

phenocrysts and the ground mass.

PG 7 is a fresh porphyrytic basalt with fine-grained ground mass and poor phenocrysts. Therefore this is somewhat similar to PG 6.

PG 9 is similar to PG 7 only with more defined phenocrysts.

PG 12 is an aphryic medium-grained basalt with occasional plagioclase microlites. The structure resembles a skeletal habitat for the plagioclase and some chlorophaeites.

PG 16 is similar to PG 12 but with much more coarse-grained basalt, both in the ground mass and other crystals.

Sample Rhyolite: Rhy is a rhyolitic ash that was obtained by Dr. Schmitt from Cove Palisades State Park in Oregon, U.S.A. This is a grey white volcanic ash with minute dark mafic crystals enclosed. This sample was analyzed as a comparison with both the mantle xenoliths and the standard USGS rock GSP-1.

II. EXPERIMENTAL

Sample Preparation

Most of the samples obtained from Dr. Robert G. Coleman had been previously separated and ground to a fine powder and then packaged in glass jars. The pyroxene samples were all hand picked crystals when we received them.

Before any activations, the samples were carefully weighed into cleaned half-dram polyvials and an effort was made to assure approximately equal sample weights to minimize any geometry problems during counting. All weighings were done in a "clean room" at the OSU Radiation Center. The vials both half-dram and two-dram, were cleaned in 6 N HNO_3, distilled H_2O, alcohol and finally the subsequent careful handling was done to prevent any contamination prior to activations. Since the samples were going to be severely jostled by the use of the pneumatic transfer system, "rabbit system", the samples were carefully packed to assure identical geometry during activation. The half-dram sample vial was first heat sealed and placed inside a two-dram polyvial. To serve as a spacer a second empty clean half-dram polyvial was then placed into the two-dram polyvial on top of the sample vial. The two-dram vial was then heat sealed. This provided a solid, leak proof vial to prevent any loss of radioactive material.

The standards for the "rabbit runs" were prepared in a similar way and were then reused. Aliquants of standards used for the high flux activations were merely pipetted into a clean half-dram polyvial with a disposable glass pipette. The vial was heat sealed and further heat sealed into a two-dram vial. No preactivation weighing of the standards was necessary since after the long activation all the standards were transferred and weighed into a clean half-dram vial for counting. Also after the long activation, the sample half-dram vials were transferred to clean two-dram vials for counting. These steps were done to eliminate further any possible radioactive contamination from the activated polyvials.

Duplicate rock standards were included in every activation as internal standards and also as primary standards. Table 1 shows the standard rocks used in each of the activations. The USGS (United States Geological Survey) rock standards used in these runs were BCR-1 (basalt), GSP-1 (granodiorite) and PCC-1 (peridotite).

The numbering systems on some of the whole rock samples were derived from the previous labeling of Dr. Coleman and further devised by D. Coles in his thesis. The bottles contained both a lab and a field number. For example:

Coleman's number	Field:	JT-45
	Lab:	M115-488-WD
My number		SAB-488

Table 1. Activation samples and standards.

Run #	Power Level (a)	Time of Activation	USGS Rock Stds Included	Samples Included
1	50 kW	2 min	BCR-1 (2), GSP-1, PCC-1	SAB 215 SAB 486 -- SAB 492 SAB 793 -- SAB 797
2	1 MW	3 hr	BCR-1 (2), GSP-1	SAB 215 SAB 486 -- SAB 492 SAB 793 -- SAB 797 PG 6A, 6B, 7A, 7B, 9A, 9B, 12A, 12B, 16A, 16B
3	50 kW	2 min	BCR-1 (2), GSP-1, PCC-1	SAB 476 -- SAB 485 SAB P486 -- SAB P492 SAB P478 -- SAB P483
4	1 MW	3 hr	BCR-1 (2), GSP-1	Same as Run 3
5	60 W 100 kW	1 min 5 min	BCR-1 (2), GSP-1, PCC-1	SAB O794, SAB C793, SAB C246, SAB C797, CP-53, CP-AHR, CP-NId, CP-SR
6	1 MW	7 hr	BCR-1 (2), GSP-1	Same as Run 5

(a) 1 kW = 3×10^9 neutrons/cm^2/sec in the O.S.U. TRIGA rotating rack.

This numbering scheme was chosen as it offered the best sequential numbering system for the samples. The SAB stands for "Saudi Arabian Basalt".

The mineral separates were numbered in a similar manner except for a prefix before the number to explain which mineral was involved. A "P" prefix means a plagioclase mineral separate, a "C" prefix means a clinopyroxene mineral separate, and an "O" prefix means an orthopyroxene separate. For example:

Coleman's number	Field: 58688 Lab: Plagioclase
My number	SAB-P479

The various types of instrumental runs used in this work were "rabbit runs" (pneumatic transfer system of the OSU Triga reactor) for short-lived isotopes and long-lived activation at 1 Megawatt (3×10^{12} neutrons/cm^2/sec) in the OSU Triga reactor rotating rack. The actual power levels and times of irradiation used are described in Table 1. Activations for the three radiochemical experiments were done at 1 Megawatt power level and for a time period of 8 hours in the rotating rack.

Elemental Analysis

The analytical work was done via sequential INAA (Instrumental Neutron Activation Analysis) and RNAA (Radiochemical Neutron

Activation Analysis). A Ge(Li) detector coupled with the Nuclear Data 2200 (2048 channel) pulse-height analyzer was used for all of the instrumental counting. A high resolution Ge(Li) detector (FWHM 2.0 keV) coupled with the Nuclear Data 3300 (4096 channel) pulse-height analyzer was used for the radiochemical REE counting. A NaI(Tl) detector coupled with a TMC 400 channel analyzer was used for the remainder of the radiochemical counting. Gordon et al. (1968) and Schmitt et al. (1970) have given a comprehensive discussion of the Ge(Li) detection using neutron activation and its application to rock analysis.

The 37 elements analyzed in this work are: by INAA; Al, Mn, Ti, V, Mg, Ca, Na, Cr, Sc, Fe, Co, Ni, Rb, Cs, Ba, La, Ce, Sm, Eu, Tb, Dy, Yb, Lu, Zr, Hf, Ta, Ir, Au, and Th and by RNAA; the REE, Ba, Sr, K, Rb, and Cs. Rubidium, Cs, and Ba, and some of the REE are repeated in the radiochemical scheme. Aluminum, Ti, V, Mg, Ca, Mn, Dy, and Na were all analyzed as a result of the "rabbit run". The remaining 21 elements of the INAA group were analyzed with an activation at 1 Megawatt (MW) (3×10^{12} neutrons/cm^2/sec) for 3 hours. The elements were counted according to the scheme shown in Table 2.

Radiochemical analysis was done to give a good check on the REE curve on a few selected samples with low REE abundances. This was done by activating a small amount of sample for 8 hours at 1 MW.

Table 2. Sequential instrumental neutron activation analysis.

Counting Sets:

1. 15 min decay, 200 sec count Ge(Li)
2. 3 hr decay, 1000 sec count Ge(Li)
3. 3 hr decay, 4 sec count NaI(Tl)
4. 1-2 day decay, 4 min count NaI(Tl)
5. 5 day decay, 2K-10K sec count Ge(Li)
6. 2 week decay, 10K-20K sec count Ge(Li)
7. 6 week decay, 20K-80K sec count Ge(Li)

Activation	Isotope	Half-life	Energy (keV)	Counting Set
50 kW for 2	Ti- 51	5.79 min	320	1
min,	Mg- 27	9.46 min	1014	1
"Rabbit Run"	V - 52	3.75 min	1434	1
	Al- 28	2.33 min	1779	1
	Ca- 49	8.80 min	3084	1
	Dy-155	2.32 hr	95	2
	Eu-152m	9.3 hr	122	2
	Mn- 56	2.38 hr	847	2,3
	Na- 24	15.0 hr	1368, 2754a	4,5
1 MW for 3	Sm-153	46.8 hr	103	5,6
hr,	Eu-152	12.7 yr	122, 1408b	5,6,7
"Long Lived"	Lu-177	6.74 d	208	5
	Yb-175	101 hr	396	5,6
	Au-198	64.8 hr	412	5,6
	Ba-131	12.1 d	496	5,6
	Nd-147	11.1 d	531	5,6
	La-140	40.2 hr	1597	5,6
	Cr- 51	27.8 d	320	6,7
	Sc- 46	83.9 d	889, 1120	6,7
	Rb- 86	18.7 d	1078	6
	Fe- 59	45.6 d	1099	6,7
	Co- 60	5.26 yr	1332	6,7
	Ce-141	32.5 d	145	7
	Tb-160	72.1 d	299	7
	Th(Pa-233)	27.0 d	312	7
	Ir-192	74.2 d	468	7
	Hf-181	42.5 d	482	7
	Cs-134	2.05 yr	605	7
	Zr- 95	65.5 d	756	7
	Ni(Co-58)	71.3 d	811	7
	Ta-182	115 d	1221	7

a 2754 keV peak not used in set 5

b 1408 keV peak not used in set 5

The activation was done in two parts, 7 hours on one day and 1 hour the second day immediately before starting the chemical work in order to reactivate the short lived isotopes. The overnight delay permitted partial decay of some unwanted isotopes such as 15-h ^{24}Na. The samples was then subjected to the scheme shown in Table 3.

The radiochemical procedure gives a better sensitivity for each element than INAA since most of the interferences are removed. The radiochemical scheme used here was obtained from discussions with Drs. J.C. Laul and W. V. Boynton, and D. B. Curtis who had previous experience with these techniques. The scheme for counting the REE and other elements from the radiochemical scheme is shown in Table 4. Chemical yields for the radiochemical scheme were determined by reactivating the sample and comparing it to an original carrier standard.

The significant activation parameters (eg. gamma ray energies, half-lives, cross sections etc.) are all catalogued by Filby et al. (1970) for the nuclides expected to result from the activation.

The following is a detailed description of the analyses and the associated errors:

Aluminum: The Al abundance was determined in all samples by two processes with equally good results. I either measured Al with a 1 min activation by counting the 1778.7 keV gamma ray from 139-s ^{28}Al after a 90 sec delay or by counting the same ^{28}Al after a 2 min

Table 3. Radiochemical scheme for rare earth elements.

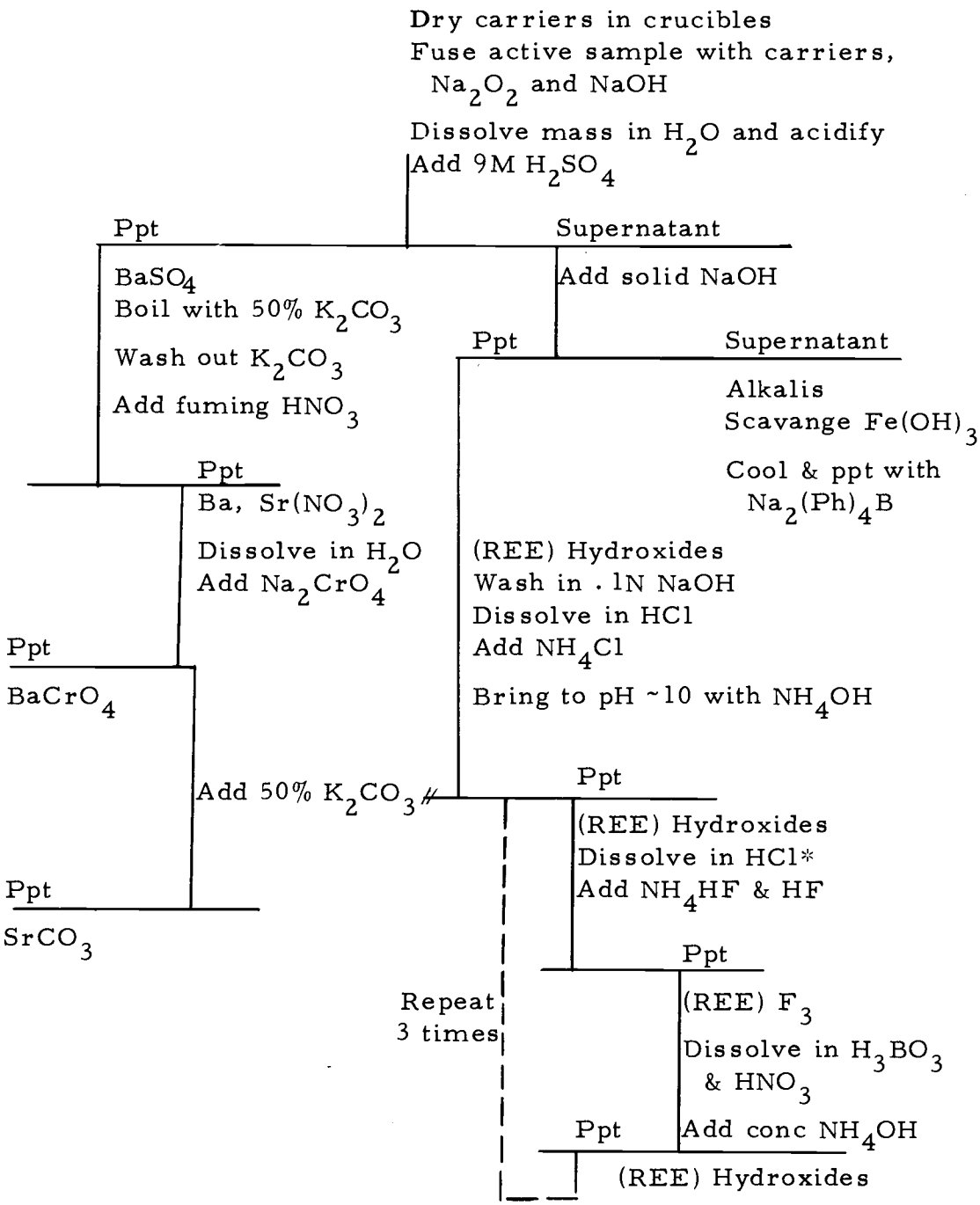

*Note: The fluoride ppt and subsequent work was done in a clear polycarbonate centrifuge tube.

Table 4. Isotopes used for group counting of REE.

Counting Sets:

1) 6-12 hours after EOB 2) 2-3 days after EOB
3) 5-10 days after EOB 4) 20-40 days after EOB

Isotope	Half-life	Energy (keV)	Counting Set
La-140	40.2 h	487.0, 1596.6	2, 3
Ce-141	32.5 d	145.5	3, 4
Pr-142	19.2 h	1575.6	2, 3
Nd-147	11.1 d	91.1	3, 4
Sm-153	46.8 h	103.2	2, 3
Eu-152	12.7 y	121.8, 344.2	2, 3, 4
Gd-153	242 d	97.5	4
Gd-159	18.0 h	363.3	2
Tb-160	72.1 d	86.8, 298.6 879.3	3, 4
Dy-165	2.32 h	94.5	1
Ho-166	26.8 h	80.6	2, 3
Er-171	7.52 h	208.3	1
Tm-170	125 d	84.3	3, 4
Yb-175	4.21 d	396.1	2, 3
Lu-177	6.74 d	208.3	2, 3

activation and 10 min decay. The sample was counted for 100 seconds on a Ge(Li) detection system to eliminate the interference of the 1811.2 keV gamma ray of ^{56}Mn. After about a 15 min decay to allow the high ^{28}Al activity to decrease, the lower activities of Ti, Mg, V and Ca were counted as noted previously by Wakita et al. (1970).

The only necessary correction was from the production of ^{28}Al by the reaction ^{28}Si(n, p)^{28}Al. The SiO_2 abundance is unknown for these samples. However, the ^{28}Si(n, p)^{28}Al correction is small (<1%). Since BCR-1 was used as a secondary Al standard, the Si correction was internally made.

The statistical error resulting from counting was from 0.5 to 1.5%. An overall error of about 2% could be expected in this method. The values of Al in all of the BCR-1 samples agreed well with the accepted value given by Flanagan (1972), Boyton (1973), Curtis (1973) and Laul and Schmitt (1973).

Titanium: Titanium was counted in the samples during the "rabbit run" after a 15 min decay. The sample was counted on an elevated shelf of the Ge(Li) detection system for 200 seconds. Titanium was detected by counting the 320.0 keV gamma ray of 5.79-m ^{51}Ti.

Counting statistics gave errors ranging from 5 to 80% depending on the type of sample being analyzed. The layered gabbros have errors of 5 to 10%. The xenoliths and mineral separates gave very

high errors due to the very low concentrations of Ti. The agreement of Ti in BCR-1 samples with those of Flanagan (1972) and others was very good.

Vanadium: Vanadium, like Ti, was counted on the Ge(Li) system for 200 seconds after allowing the ^{28}Al activity to decay appreciably. Vanadium was determined by counting the 1434.3 keV gamma ray from 3.75-m ^{52}V. This peak sits on the large Compton edge which results from the 1778.7 keV gamma ray of ^{28}Al. Since the half-lives of both isotopes are comparable, the peak must be carefully selected.

Vanadium abundances were not obtained for all samples due to the low V abundances in some samples. The statistical uncertainties ranged from 5 to 10%. Agreement of BCR-1 values was good as shown in Table 5.

Magnesium: Magnesium, like the two previous elements Ti and V, was counted on the Ge(Li) system for 200 seconds after a 15 min decay. Magnesium was counted by using the 1014.5 keV gamma ray from 9.46-m ^{27}Mg. This is a very easy element to determine since Mg is in the percent range. I did not obtain values for all of the samples due to printing errors for some samples.

The statistical errors for the samples ranged from 1 to 10%. The values for BCR-1 standard rocks agreed well with those of Flanagan (1972). A correction must be made on all Mg values due to

Table 5. Table of the BCR values of INAA.

Element	BCR-1A	BCR-1B	BCR-1C	BCR-1D	BCR-1E	BCR-1F	Average	Laul & Schmitt (1973)	Flanagan (1972)
	Run 2		Run 4		Run 6				
(%)									
TiO_2	2.25	2.05	2.40	1.96	2.21	2.17	2.18	2.20	2.20
Al_2O_3	13.2	13.6	14.0	13.7	13.6	13.7	13.6	13.7	13.61
FeO	12.5	12.1	12.5	12.2	12.1	12.2	12.3	12.3	12.3
MgO	2.96	4.06	3.00	3.86	3.37	3.50	3.46	3.3	3.46
Na_2O	3.30	3.31	3.29	3.18	3.30	3.32	3.28	3.30	3.27
CaO	6.62	6.10	7.20	6.13	6.94	6.87	6.64	6.8	6.92
MnO	0.168	0.170	0.185	0.207	0.187	0.177	0.182	0.176	0.18
(ppm)									
Cr_2O_3	16.0	19.1	23.1	16.7	18.0	19.1	18.7	18.0	22.0
Sc	(a)	(a)	(a)	(a)	34.6	34.3	34.5	32	33
Co	(a)	(a)	36.5	37.1	37.5	38.8	37.5	36	38
V	402	405	406	395	407	401	403	410	399
Ba	637	590	(b)	(b)	754	516	624	590	675
Cs	(a)	(a)	1.04	1.03	0.89	1.02	1.00	--	0.95
Th	5.8	6.1	5.7	5.8	6.1	6.0	5.9	5.5	6.0
Zr	185	192	191	177	221	203	195	--	190
La	25.9	25.5	25.5	24.6	25.9	26.3	25.6	25.5	26
Ce	51.6	51.2	54.0	53.2	52.4	54.2	52.8	53	53.9
Sm	6.79	6.77	7.04	6.74	6.73	6.91	6.83	6.9	6.6
Eu	(a)	(a)	1.83	2.07	1.82	1.97	1.92	1.95	1.94
Tb	1.20	1.10	1.03	1.17	1.02	1.12	1.11	0.96	1.0
Dy	6.7	6.2	6.2	6.9	6.3	6.7	6.5	6.4	6.3
Yb	3.20	3.57	3.43	3.42	3.12	3.43	3.36	3.4	3.36
Lu	0.50	0.55	0.57	0.54	0.55	0.57	0.56	0.55	0.55
Hf	4.8	5.1	4.6	5.0	4.6	4.8	4.8	4.7	4.7
Ta	0.95	0.83	1.27	0.72	0.75	0.94	0.91	0.77	0.91

(a) BCR-1 used as STD. (b) Ba was not determined in Run 4.

the reaction of $^{27}Al(n,p)^{27}Mg$. This correction, which can be important in the high plagioclase minerals, turns out to be 0.35% Mg for each 1% Al in the sample. Based on a comparison with data reported by Coleman et al. (1973) an overall uncertainty of between 5 to 40% was estimated for the samples.

Calcium: Calcium, like the previous group Ti, V and Mg, was counted for 200 seconds on the Ge(Li) system after a delay for Al activity decay. The gamma ray used is the 3100 keV gamma ray for 8.8-m ^{49}Ca. The counting of this element was not ideal due to the very high energy gamma ray and the low efficiency of counting at the high energy end of the spectra.

Counting and overall errors ranged from 5 to 20% for the samples. BCR-1 values agreed well with the ones listed in the literature.

Manganese: Manganese abundances were determined in the samples during the "rabbit runs" along with the Eu and Dy. After a delay of about 3 hours, to allow decay of the short-lived isotopes (Al, Ti, V, Mg, and Ca) Mn was determined by counting the 846.7 keV gamma ray of 2.56-h ^{56}Mn. The ^{56}Mn was counted along with Eu and Dy on the Ge(Li) detection system. Simultaneously, ^{56}Mn was also counted for 1 min at an elevated shelf using a 7.6 cm x 7.6 cm NaI(Tl) detector to eliminate any geometry errors. The counting uncertainties were as low as 0.5 to 1.0%. The Mn values of BCR-1 agreed well with Flanagan (1972) and Laul and Schmitt (1973).

Sodium: The INAA for Na was ideal. Sodium was counted for 4 minutes on the NaI(Tl) detector from the "rabbit run" after about a 2 day decay. By counting the sample in the well one assures almost identical counting geometries. There were no interferences involved with counting the 1368.4 keV gamma ray of 15.0-h ^{24}Na.

Sodium was again counted after the 3 hr activation at 1 MW for 1000 seconds at a high (~21 cm distance) geometry. The count rate here was again high and the statistics were very good. Counting of Na was repeated in order to test the precision of analysis.

The uncertainties obtained for the Na abundances were about 1% for the samples. Sodium has two corrections to the abundances values that must be accounted for before the true value can be obtained. ^{24}Na can be produced by the reactions $^{24}Mg(n, p)^{24}Na$ and $^{27}Al(n, \alpha)^{24}Na$. The correction for Mg is about 10^{-3}% Na for each 1% Mg. This may be considerable if Mg is in the high percent range and Na, in the tens of ppm level. The correction for Al was about 6×10^{-3}% of Na for each 1% Mg. This will bring the overall uncertainty for Na to about ±2%.

BCR-1 values agreed well with the other published works. In the long activation one of the rock standards (BCR-1) was used as a standard because of its greater accuracy and ease of counting.

Chromium: The single gamma ray at 320.1 keV of 27.8-d ^{51}Cr was counted after a six week decay. Little or no interference was

found from other gamma rays although ^{232}Th (^{233}Pa) is nearby at 311.9 keV. One can usually tell the difference between the two peaks unless the ^{51}Cr peak is so large that it overflows onto the ^{233}Pa peak. Chromium is counted twice as a check on the accuracy of the various counting sets. The agreement is good but the last count is more accurate for BCR-1.

Statistical uncertainties ranged from 1 to 25% depending on the Cr content in the sample. The values of BCR-1 agreed well with those stated by Flanagan (1972).

Iron: Iron is quite an easy element to determine by INAA. It is a major element in the rock samples and is easily activated to a long-lived isotope. One uses the 1099.3 keV gamma ray of 45.6-d ^{59}Fe for analysis.

Iron was counted six weeks after activation for 20K or 40 K seconds on the Ge(Li) detection system. The statistical uncertainties were usually below 1% for the Fe values. The value of BCR-1 was in very good agreement with the published values with almost no variations in the various analysis as shown in Table 5.

Cobalt: Cobalt provided two of the most prominent peaks in a rock sample gamma ray spectra after a six week decay. Cobalt could be detected by using either the 1173.2 keV or 1332.5 keV gamma ray from 5.26-y ^{60}Co. The 1332.5 keV gamma ray peak was used for this work since it was an interference free peak. This has a very

easy and trustful abundance value to consider in the analysis. This element was again counted twice to check the accuracy of the system with good results.

The uncertainties ranged from 1 to 3% for the abundance values. Agreement with Flanagan (1972) and Laul and Schmitt (1973) for the BCR-1 values was good. Variations for the BCR-1 values were very minimal.

Scandium: ^{46}Sc presents the most prominent photo peak in the gamma ray spectra taken after a two week decay. The isotope 83.9-d ^{46}Sc emits two equally strong gamma rays at 889.3 and 1120.5 keV.

Both of the gamma rays have interference problems. The 889.3 keV gamma ray sits on the Compton edge from the 1120.5 keV gamma ray peak. The 889.3 keV has some small interferences from the 871.9 keV gamma ray of 72.1-d ^{160}Tb. Since Sc follows the REE in many cases, there will be less interference from the ^{160}Tb when the Sc abundance is high. This problem can be overcome by carefully choosing the peak limits and background during the peak integration. The 1120.5 keV gamma ray peak was interfered with by the 1115.5 keV peak from 243-d ^{65}Zn. This is the only gamma ray emitted by ^{65}Zn so no correction ratio can be obtained.

For the above reasons both ^{46}Sc peaks were analyzed and the one with less interferences was used. For a double check Sc was counted with a Ge(Li) detector in both the two and six week counts.

The statistical uncertainties on the Sc values were small at about 1%. The values obtained for BCR-1 agreed well with those of Flanagan (1972).

Thorium: The Th determination relies on the following decay chain:

$$^{232}\text{Th} + n \rightarrow {}^{233}\text{Th} \xrightarrow{22\ \text{m}} {}^{233}\text{Pa}^{*} \xrightarrow{27.0\text{-d}} {}^{233}\text{Pa} + 312\ \text{keV}\ \gamma\text{-ray}$$

The Th content was measured by determining the 311.9 keV gamma ray of 27.0-d ^{233}Pa. Thorium, like Fe, was counted six weeks after activation for 20K or 40K seconds.

Thorium determination has an interference problem from the 307.5 keV gamma ray of 31.8-d ^{169}Yb, but it can be resolved well enough by carefully choosing the peak limits and background to only give a 5% error in the Th. The main interference problem for Th comes from the 320.1 keV gamma ray of 27.8-d ^{51}Cr. If the Cr content is high the low energy side of the ^{51}Cr peak may cover the ^{233}Pa peak. This has been observed in some of the samples. Also this overflow of ^{51}Cr over the ^{233}Pa peak will cause some problems with the Th correction on the Tb content. The excellent agreement with the BCR-1 values gave a good confidence in the determined Th values. GSP-1 was used as a primary Th standard as it has a high Th content of 110 ppm. This gives much more reliable results than a pure Th standard.

The uncertainties on the Th values ranged from 3 to 50% depending on the Cr content and the Th content. The average uncertainty was between 10 to 20%.

Hafnium: The main problem with determining Hf was its low abundance and hence its low activity. Hafnium was determined six weeks after activation by means of the 482.2 keV gamma ray of 42.5-d ^{181}Hf. It was counted this late to allow for the decay of 487.0 keV gamma ray of 40.2-h ^{140}La. Uncertainties for Hf ranged from 3 to 20%. Hafnium was observed in almost all of the samples. The Hf values for BCR-1 agreed well with those of Flanagan (1972).

Tantalum: Tantalum was a difficult element to detect due to its low activity and the high energy gamma ray. GSP-1 was used as the Ta standard since a good standard is hard to obtain. The observed value for BCR-1 was well within experimental error of the value cited by Flanagan (1972). Tantalum was detected by counting the 1221.3 keV gamma ray of 115-d ^{182}Ta six weeks after activation. Uncertainties ranged from 10 to 50% for the samples. Tantalum was observed in most samples.

Zirconium: Zirconium determination was hampered principally by the low activation parameters. Zirconium was obtained six weeks after activation by means of the 756.0 keV gamma ray of 65.5-d ^{95}Zr. The samples were counted for 20 to 80K seconds to obtain good results on the Ge(Li) detection system.

Zirconium abundances were not obtained in all samples due to the large uncertainties and low abundances. The uncertainties for those values obtained were from 20 to 80%, which gave a large deviation in the sample groups. The values for BCR-1 were well within experimental error of those given by Flanagan (1972) and Laul and Schmitt (1973).

Iridium: Iridium values were obtained for the samples in Run 6 only because no standard was used in the earlier runs. Since Ir is heterogeneously present in BCR-1 and GSP-1, it was not safe to use these rocks as appropriate standards.

Iridium was detected by counting the 468.1 keV gamma ray of 74.2-d ^{192}Ir. This peak was clean but the values obtained were near the lower limit of detection.

Gold: Gold was only obtained in Run 6 since no appropriate standard was used in either Run 2 or Run 4. None of the standard rocks had a reliable enough value cited in the literature to allow their use as a standard. Gold is known as a heterogenous element in most rock samples due to its very low abundance (ppb range) and therefore the agreement of BCR-1 values with those of Flanagan (1972) was only within experimental error. Gold was also not seen in the first two runs due to the shorter activation time used.

Gold was determined using the 411.8 keV gamma ray of 64.8-h ^{198}Au. This peak has only one interference from ^{152}Eu.

Uncertainties for the abundances ranged from 2 to 20% with 10 to 15% as the more common range.

Rubidium: The analysis for Rb was marginal since it bordered on the lower limits of detection for the instrumental portion of the analysis. Rubidium abundances were obtained more accurately through the radiochemical scheme.

In the instrumental run Rb was not detected in all of the samples. Where Rb was observed, it was by means of the 1078.8 keV gamma ray of 18.7-d ^{86}Rb. The measured Rb abundance values for BCR-1 agreed well with those given by Flanagan (1972). No interference was noted in the counts six weeks after activation by using the Ge(Li) detection system.

In the radiochemical scheme, Rb was easily measured by counting the same 1078.8 keV gamma ray peak after Rb was separated from the sample. Rubidium was precipitated with Cs and K, and must be counted on the Ge(Li) detection system due to the low count rate. The statistics on Rb values gave uncertainties ranging from 10 to 20%. The values on BCR-1 from the radiochemistry agreed very well with those of Flanagan (1972) and Laul and Schmitt (1973).

Cesium: The analysis for Cs was good in most samples by the instrumental scheme. The values were just above the detection limit so it was possible to get good values. The values from the radiochemical scheme were much better statistically.

Cesium was detected in the samples by counting 605.0 keV gamma ray of 2.05-y ^{134}Cs. The peak was interference free with a Ge(Li) detection system. The values obtained for BCR-1 agreed with those of others as shown in Table 5.

By means of radiochemical separation Cs, like Rb, was easy to count after precipitation. Cesium was counted on the Ge(Li) system for the necessary resolution of the 605.0 keV gamma ray peak of 2.05-y ^{134}Cs from the tracer peak at 662.0 keV of ^{137}Cs. Values for BCR-1 agreed well with Laul and Schmitt (1973). Statistical uncertainties for Cs were 10 to 15% on the instrumental run and 5 to 8% on the radiochemical separation.

Nickel: The Ni determination relies on the activation reaction: $^{58}Ni(n, p)^{58}Co$. By the use of the 811.1 keV gamma ray of 73.1-d ^{58}Co, I was able to measure the Ni content. The peak was free from interferences.

Accurate Ni determinations were hampered by the low Ni content in the rocks and the heterogeneity of the element. The statistical uncertainties of the Ni values were from 10 to 50%. The values obtained for BCR-1 were within the limits given by Flanagan (1972) and Laul and Schmitt (1973).

Lanthanum: Lanthanum, like some of the other REE, was determined both instrumentally and radiochemically. In both determinations, the values for La were equally good using the 1596.6 keV

gamma ray peak of 40.2-h ^{140}La. This was a very pure peak with no interferences. In the radiochemical counting I also used the 487.0 keV gamma ray of ^{140}La.

Instrumentally, La was counted twice, once after a 5 day decay and again after two weeks of decay. With the samples being counted twice, the agreement was good between the two counts. The agreement of La in BCR-1 compared well with the given literature values. The statistical errors given for La were 5 to 10%.

The La chemical yields were depleted due to the fluoride precipitations in the radiochemical scheme. Even with this loss, excellent results and very good counting statistics were obtained. The determination of La by this means gave statistical uncertainties of 1 to 3%.

The agreement of values between the INAA and RNAA were very good and agreement of BCR-1 gave excellent dependence on the La values.

Cerium: Cerium was determined both instrumentally and radiochemically. The isotope was counted using the 145.5 keV gamma ray of 32.5-d ^{141}Ce. Instrumentally the samples were counted six weeks after activation to allow for a lower background. The 145.5 keV gamma ray peak has some interference from the 143.0 keV gamma ray peak of 45.6-d ^{59}Fe. Since the half-lives of the two elements are comparable, the only way to correct for the interference

is by the ratio of the 143 to 1099 keV photo peaks of ^{59}Fe. Cerium also has about a 1.5% correction for the Th content of the rock. In some of the pyroxene samples, I was not able to make the Th correction due to high Cr; this caused the actual Ce values to be very high and unreliable for use in this work. This correction was usually minor compared to the Fe correction. With these subtractions, I obtained an error of 10 to 15% for Ce. The agreement shown in Table 5 on BCR-1 values was better than expected. The values for the pyroxene samples were completely overshadowed or erratic due to the Fe and Th content.

In the radiochemical scheme, Ce was very easy to determine and gave counting statistics of 3 to 10% error. As can be seen in the REE curves, the radiochemical Ce values agreed much better than by the instrumental methods. Cerium counting in the radiochemical scheme was done one to three weeks after separation for the best values.

Praseodymium: Values for Pr were somewhat unsure and were not obtained in all of the samples that underwent radiochemical separation. Praseodymium values were obtained by counting the 1575.6 keV gamma ray peak of 19.2-h ^{142}Pr. Counting statistics gave very large errors (10 to 30%) for most of the samples. This element was hard to determine due to the high energy of the gamma ray and the short counting periods of the first counts.

Neodymium: Neodymium was attempted instrumentally in the samples. The statistical errors and half life check precluded the use in this work. Abundances would only be possible in samples with highly abundant light REE and since all of the gabbros tend to show REE numbers about equal to the chondritic values, I could not use the Nd values.

Neodymium was counted using the 531.0 keV gamma ray of 11.1-d ^{147}Nd. The statistical errors ranged from 25 to greater than 100%, which can not be accepted as very precise. The Nd values from the two instrumental determinations gave varying numbers and prompted a half-life check on the values that were acceptable. The check proved that what I was actually detecting was not pure Nd. The measured values for BCR-1 instrumentally were not in good agreement so I was not able to use Nd values from the instrumental run.

In the radiochemical run, Nd was counted using the 91.1 keV gamma ray from 11.1-d ^{147}Nd. Values were obtained for all but SAB C797 in the radiochemical scheme. The values obtained in this process were very good and agreed well with other REE in the various curves presented. The statistical errors on the values were very good and BCR-1 values agreed well with the literature values.

The samples were counted two or three days after separation for the best results. They were counted on the high resolution Ge(Li) system to separate the low energy peak from the other REE photo peaks.

Samarium: Like La, very good Sm values were obtained by both instrumental and radiochemical methods of analysis. This element shows up very well early in all of the counting sequences by using the 103.2 keV gamma ray of 46.8-h ^{153}Sm. In the instrumental work Sm was counted five days after activation for 2K to 10K seconds depending on the overall activity of the sample. The values have statistical errors of 5 to 10%.

In doing the radiochemical counting I had problems because the Sm activity was so high and I had to let this activity subside before I could count the other long lived REE. The statistical errors on the Sm values were from 1 to 5%. The Sm abundance in BCR-1 compared well with those given by Flanagan (1972) and Laul and Schmitt (1973).

Europium: Europium was easily measured in all samples. Europium as counted in all of the runs as an internal check. This element was counted during the "rabbit run" by using the 121.8 keV gamma ray of 9.3-h ^{152m}Eu. This can be easily measured during the short activation with little interference from the 121.8 keV gamma ray of 12.7-y ^{152}Eu. The Eu was counted along with Mn and Dy for 200 seconds after a 3 hr decay. The statistical error here was much higher than any other counting period and it was used only as a check.

Europium was again counted after the high neutron flux-intensity activation in three counting sets; one count after five days, the second count after one to two weeks, and the third after six or

more weeks of decay. The Eu was counted by using the 121.8 keV and 1408.1 keV gamma rays of 12.7-y ^{152}Eu. The former energy was not valid in the first count due to the interference of 121.8 keV gamma ray of 9.3-h ^{152m}Eu. The second count may have been free of interference and the third was definitely pure. With the 1408.1 keV gamma ray I had no interference and any counts accumulated at that high energy was all ^{152}Eu. The problem of low efficiency of the detector at the high energies was no real problem due to the ease of activation of Eu.

In the radiochemical scheme Eu was again obtained in all of the counts. Europium was determined by using the 121.8 keV and 344.2 keV gamma rays of 12.7-y ^{152}Eu. The determination in the first count was again plagued by the 9.3-h ^{152m}Eu in the 121.8 keV gamma ray peak. The second peak and the later counts on the lower energy peak were all good and gave agreeable results. The counting statistics were very good on all of the runs.

Gadolinium: The values for Gd, where obtained, were done by means of the radiochemical scheme. The values were not reliable for all of the samples because the counting was not ideal for the half-life of the isotope that I used. Gadolinium was counted by using either the 363.3 keV gamma ray energy peak of 18.0-h ^{159}Gd or the 97.5 keV gamma ray peak of 242-d ^{153}Gd. The first peak has the same problem as was noted for Pr. I was not able to use the second peak as I

was unable to wait the three to four weeks necessary for good statistics in the peak.

The statistical uncertainties on Gd values were 10 to 20%. The BCR-1 values were within the statistical errors.

Terbium: Terbium was best detected in the last counts of both the instrumental and radiochemical analysis due to the long half-life. In the instrumental sequence Tb was detected by the use of the 298.6 keV gamma ray peak of 72.1-d ^{160}Tb. This was not a pure peak because Th has an interfering secondary peak at 299.0 keV. A correction was made by taking the ratio of the 299.0 peak: 311.9 peak and making the necessary subtraction from the Tb peak. This correction may be up to 40% of the Tb peak when the values are very low. The statistical error for Tb was 10 to 30%. The agreement of the BCR-1 values is shown in Tables 5 and 6.

In the radiochemical sequence I counted Tb by using the 86.8 keV gamma ray peak, the 298.6 keV gamma ray peak, and the 879.3 keV gamma ray peak of 72.1-d ^{160}Tb. The peaks were all good in the later counts but only the last two were used in the first few counts. The statistics were good (5 to 15%) in this determination and I believe the values are reliable. The position of the values in the REE curves and the agreement with the BCR-1 values also tend to show good reliability. The first of the peaks (86.8 keV) was not as good in the first counts due to the many surrounding REE peaks.

Table 6. Elemental abundances from RNAA.

	SAB C797	SAB P489	SAB 793	SAB 797	SAB 482	SAB 489	BCR - 1 Ave of 3	1a	2b
K	860	590	—	45	1310	1050	1.66%	1.68%	1.70%
Rb	2.7	0.3	<0.7	<0.1	2.5	2.1	42	—	46.6
Cs	<0.22	0.021	0.021	0.017	0.20	0.21	0.93	0.95	0.95
Ba	—	877	46	90	100	36	680	600-700	675
Sr	23.7	1700	6.4	35	887	193	320	—	330
La	0.27	1.66	0.38	1.10	3.72	1.85	26.0	25.5	26
Ce	—	2.80	0.58	4.72	10.1	6.04	54.0	53.9	53.9
Pr	—	0.35	0.09	0.84	1.41	0.70	6.65	—	7
Nd	—	1.59	0.28	5.06	7.68	3.96	28.2	29	29
Sm	0.53	0.42	0.09	1.68	2.57	1.37	6.60	6.95	6.6
Eu	0.32	1.95	0.04	0.72	1.63	0.80	1.91	1.95	1.94
Gd	0.88	0.35	0.11	2.24	2.66	2.06	6.54	—	6.6
Tb	0.18	0.06	0.02	0.34	0.30	0.37	1.01	0.96	1.0
Dy	—	0.28	0.10	2.16	1.98	1.88	6.3	6.9	6.3
Ho	0.30	0.06	0.03	—	0.28	0.42	1.17	—	1.2
Er	0.71	0.13	0.07	1.12	1.18	0.90	3.57	—	3.59
Tm	0.16	—	0.01	0.15	0.16	0.16	0.62	—	0.6
Yb	0.56	0.15	0.07	1.00	0.86	0.96	3.35	3.55	3.4
Lu	0.075	0.02	0.01	0.14	0.11	0.19	0.55	0.55	0.55

1a Laul & Schmitt (1973)

2b Flanagan (1972)

Dysprosium: This element was detected in the samples during the "rabbit run" along with Mn after a 3 hr decay, to allow for the decay of all of the short-lived elements. This element was hard to determine as it has a very low energy gamma ray and low abundance. Dysprosium was counted when there was high activity in the sample. Dysprosium was counted using the 94.5 keV gamma ray from 139-m ^{165}Dy. The group of elements Dy, Eu and Mn, were counted via INAA for 800 seconds on the Ge(Li) detection system.

Dysprosium was easily analyzed by means of the RNAA procedure outlined previously. In the RNAA procedure the group separated REE were counted for 40 to 200 minutes on the Ge(Li) system with very high resolution. In this first count of the series I was able to obtain Dy up to 12 hours after the end of activation. The statistics for Dy from the radiochemical scheme were not very good, (10 to 20%).

Holmium: Holmium was detected only in the radiochemical separation method. By counting the sample two or three days after separation, Ho values were easily determined by using the 80.6 keV gamma ray peak of 26.8-h ^{166}Ho. This peak was separated from the other low energy REE peaks with the aid of a high resolution Ge(Li) detection system.

The values obtained for this isotope seemed good with a statistical error of 5 to 10%. The agreement of BCR-1 values with those cited by Flannagan (1972) was good and the positions in the REE

curves were reasonably good.

Erbium: Erbium, like some of the other REE, was obtained only after the separation in the radiochemical scheme. This element was determined by using the 208.3 keV gamma ray peak of 7.52-h ^{171}Er. This peak was free of interferences and was easily seen in the first day of counting. The uncertainties for this element were 5 to 15% and the agreement with BCR-1 value was very good. This element, like Dy, had to be obtained in the first day of counting.

Thulium: The peak of 84.3 keV gamma ray of 125-d ^{170}Tm was very difficult to resolve since the peaks of Ho and Tb surround it. Thulium was best counted after three or four weeks of decay. The statistical errors were reasonable (20 to 30%) and BCR-1 values were within the statistical errors.

Ytterbium: Values for Yb were determined by both INAA and RNAA. The agreement between the two schemes seem to be very reasonable. Ytterbium was detected four or five days after activation in both series by the use of the 396.1 keV gamma ray peak of 4.21-d ^{175}Yb. The statistical uncertainties for INAA were 10 to 20% while for RNAA they dropped to 5 to 10%. The values for BCR-1 were in good agreement as shown in Tables 5 and 6.

Lutetium: The Lu values by INAA were obtained for all samples, but they were not as reliable as some of the other REE. This was due to the fact that the Lu peak fell on the Compton edge of ^{46}Sc and I

could not correct completely for this interference. Lutetium was analyzed by using the 208.3 keV gamma ray peak of 6.74-d ^{177}Lu. The statistical uncertainties for Lu were 10 to 20%. The agreement of BCR-1 values with those listed by Flanagan (1972) was good.

By using the radiochemical separations, the values for Lu improved greatly. The statistical errors were 3 to 7% and the agreement with the accepted BCR-1 values was good. The interference from Sc was almost completely eliminated by the radiochemical separation.

Potassium: Potassium was obtained in the radiochemical scheme along with the other two alkalis, Rb and Cs. This element was easy to obtain and should be very pure for counting if all ^{24}Na is removed. Potassium was counted by means of the 1525 keV gamma ray of 12.4-h ^{42}K. The samples were counted in the well of the NaI(Tl) detection system for 10 to 40 minutes.

Statistical uncertainties for this element ranges from 1 to 10% with 1 to 5% as the most common. The values of BCR-1 agreed well with those given by Laul and Schmitt (1973) and Flanagan (1972) as seen in Table 6.

Barium: The analysis for Ba was marginal and often bordered on the lower limits of detection for the instrumental portion of the analysis. Barium abundances were very easy to determine in the radiochemical scheme. In the instrumental run Ba was detected by

using the 496.3 keV gamma ray of 12.1-d ^{131}Ba. No significant interferences were observed in the count two weeks after activation.

In the radiochemical scheme Ba may have an interference from 478 keV ^{140}La peak if a NaI(Tl) detector is used. A 126.0 keV gamma ray from ^{131}Ba can be used also if counting with the Ge(Li) detector is necessary as during the radiochemical scheme. This peak was completely free from interferences when the separation was performed.

The uncertainties for Ba analysis ranges from 10% to as much as 100% in the abundance values, with the higher values obtained in the INAA portion. The statistical uncertainty was very dependent on the actual sample abundance as Ba is near the limit of detection. The values for BCR-1 were well within the range given by Flanagan (1972).

Strontium: The analysis of Sr was done radiochemically through the scheme outlined previously in Table 3. By chemically separating Sr from the sample it was easy to count the 388.1 keV gamma ray of 170-m ^{87m}Sr. Strontium was counted in the well of the NaI(Tl) detection system. Since the 388.1 keV gamma ray peak is free of interferences the low resolution of the NaI(Tl) detector was no problem. Statistical uncertainties ranged from 1 to 5% for the Sr values. The agreement of BCR-1 with the literature values was very good. Strontium was only obtained in the nine samples that were used in the radiochemical scheme.

III. RESULTS

Elemental Results

The analytical methods in this study are discussed in a previous section. The final results are tabulated in Tables 6 and 7. The pertinent petrographic rock type and location of each sample are also included in the tables. The average BCR-1 values are included along with the percent errors.

The basis for the correlations used in the elemental discussion is that a correlation means an agreement at the 95% confidence level by use of linear regression analysis. A positive correlation means that if one element increases or decreases then the second one will follow the trend. If the two elements act in exactly opposite ways of increases and decreases then it is called a negative correlation.

The accuracies of the analyses are best shown in Table 5 which shows the determination of all BCR-1 samples and their average as compared to the other literature values.

Titanium: According to Goldschmidt, Ti is a lithophilic element that has a strong affinity for nonmetals other than oxygen and sulfur. Titanium is known to be replaced by V and may also be associated with trace amounts of divalent Mg, Ni, Co, Zn, and Mn. These later trace elements replace the divalent Fe in the major Ti mineral, ilmenite ($FeTiO_3$). Titanium may also be found as a trace element in

Table 7. Elemental abundances by INAA.[a]

Sample #	Sample Description	TiO_2 (%)	Al_2O_3 (%)	FeO* (%)	MgO (%)	Na_2O (%)	CaO (%)	MnO (%)	Cr_2O_3 (ppm)	Sc (ppm)	V (ppm)	Co (ppm)	Zr (ppm)	Hf (ppm)
	Jabal Shayi (JS)													
SAB 485	Chillzone	1.0	14.7	10.4	11	1.00	13	0.190	1340	32	230	95	--	1.2
SAB 483	JS Chillzone	1.0	14.8	6.7	6	2.39	14	0.123	260	41	235	44	--	0.8
SAB 478	JS 0 m	1.1	22.9	6.6	3	3.62	13	0.074	90	12	300	29	--	0.4
SAB 480	JS 147 m	0.7	21.1	5.3	5	2.68	13	0.101	345	21	120	35	--	1.1
SAB 476	JS 440 m	0.4	22.5	4.7	3	2.19	17	0.087	170	21	---	36	--	0.5
SAB 481	JS 583 m	1.0	19.0	10.1	6	2.36	13	0.156	180	31	375	54	--	0.5
SAB 484	JS 901 m	0.5	18.5	5.7	--	1.59	16	0.112	1380	33	150	45	--	0.6
SAB 477	JS 1270 m	1.8	20.0	8.0	--	3.73	10	0.188	260	26	65	12	--	2.8
SAB 482	JS 1559 m	1.7	18.0	10.5	--	2.36	14	0.149	190	35	360	40	--	1.1
SAB 479	JS 2316 m	0.6	19.5	6.2	4	1.63	16	0.109	1040	34	170	40	--	0.8
	Plagioclase													
SAB P478	Separate	0.2	28.3	0.36	--	4.83	8	0.007	3	0.3	---	2.2	--	0.06
SAB P479	"	---	31.8	0.49	--	2.97	--	0.013	5	0.4	---	1.8	--	0.05
SAB P480	"	---	32.3	0.45	--	4.63	20	0.009	5	0.3	---	2.5	--	0.09
SAB P481	"	0.3	31.3	0.38	--	4.42	13	0.006	4	0.3	---	0.8	--	0.06
SAB P482	"	0.2	31.3	0.44	--	4.49	--	0.007	2	0.3	---	2.1	--	0.04
SAB P484	"	---	32.9	0.49	--	2.94	15	0.010	2	0.4	40	1.9	--	0.05
	Jabal at Turf (JT)													
SAB 215	Chillzone	1.7	17.4	11.6	6	2.50	9	0.178	65	26	280	47	--	3.6
SAB 487	JT 318 ft	0.6	18.2	8.0	7	2.07	10	0.135	700	34	170	44	--	1.0
SAB 489	JT 2212 ft	0.8	15.5	8.9	9	1.86	10	0.168	640	43	220	50	--	1.0
SAB 491	JT 5600 ft	0.2	21.2	6.3	5	1.95	11	0.108	240	13	70	42	--	0.13
SAB 492	JT 5600 ft	0.9	15.0	9.6	5	1.90	12	0.173	670	57	380	45	--	1.1

Table 7. Continued.

Sample #	Th (ppm)	Ta (ppm)	Ba (ppm)	Cs (ppm)	Ir (ppb)	Ni (ppb)	Au (ppb)	La (ppm)	Ce (ppm)	Sm (ppm)	Eu (ppm)	Tb (ppm)	Dy (ppm)	Yb (ppm)	Lu (ppm)
SAB 485	0.17	0.07	--	0.06	--	--	--	4.2	10.9	1.76	0.86	0.33	2.3	1.2	0.18
SAB 483	0.23	0.02	--	--	--	--	--	2.1	4.8	1.92	1.13	0.27	0.9	0.4	0.05
SAB 478	0.18	0.02	--	--	--	--	--	2.3	3.4	0.88	1.22	0.13	0.7	0.2	0.04
SAB 480	0.23	0.11	--	0.15	--	--	--	4.6	10.4	1.68	1.00	0.22	1.1	0.5	0.06
SAB 476	0.17	0.08	--	<0.03	--	--	--	2.0	4.4	1.08	0.77	0.18	1.0	0.4	0.05
SAB 481	--	0.07	--	0.09	--	--	--	1.8	5.3	1.25	0.71	0.23	0.8	0.4	0.05
SAB 484	0.11	0.04	--	<0.05	--	--	--	2.4	7.0	1.53	0.80	0.27	1.6	0.6	0.09
SAB 477	0.19	0.21	--	0.17	--	--	--	6.4	14.7	3.92	2.13	0.78	4.5	3.0	0.40
SAB 482	0.23	0.04	--	0.15	--	--	--	3.7	11.0	2.77	1.71	0.39	2.2	0.8	0.10
SAB 479	0.13	<0.01	--	--	--	--	--	2.1	7.5	1.61	0.85	0.22	1.4	0.5	0.07
SAB P478	0.05	0.03	--	0.04	--	--	--	2.8	5.2	0.65	11.61	0.09	---	0.3	0.04
SAB P479	0.02	0.01	--	0.02	--	--	--	2.7	4.8	0.59	6.42	0.09	---	0.2	0.04
SAB P480	0.05	0.03	--	--	--	--	--	5.3	8.8	1.06	12.19	0.18	---	0.4	0.05
SAB P481	0.03	0.02	--	0.04	--	--	--	2.3	4.6	0.64	6.21	0.08	---	0.3	0.04
SAB P482	0.03	0.01	--	0.06	--	--	--	3.5	6.9	0.73	9.93	0.09	0.5	0.3	0.04
SAB P484	0.02	0.01	--	--	--	--	--	1.0	1.9	0.24	4.60	0.04	0.3	0.1	0.02
SAB 215	0.33	0.50	90	0.25	--	--	--	7.6	19.8	4.14	1.54	0.74	3.5	2.0	0.33
SAB 487	0.24	0.21	--	0.13	--	--	--	2.3	5.8	1.32	0.69	0.33	1.6	0.9	0.22
SAB 489	0.22	0.22	--	0.16	--	--	--	2.0	6.0	1.38	0.64	0.30	2.1	1.2	0.21
SAB 491	0.11	0.03	--	0.07	--	--	--	0.9	2.6	0.41	0.40	0.04	0.5	0.3	0.05
SAB 492	0.22	--	--	0.12	--	--	--	2.0	6.2	1.54	0.74	0.33	2.0	1.3	0.26

Table 7. Continued.

Sample #	Sample Description	TiO_2 (%)	Al_2O_3 (%)	FeO* (%)	MgO (%)	Na_2O (%)	CaO (%)	MnO (%)	Cr_2O_3 (ppm)	Sc (ppm)	V (ppm)	Co (ppm)	Zr (ppm)	Hf (ppm)
	Plagioclase													
SAB P486	Separate	0.3	30.7	0.80	--	4.22	15	0.013	3	0.4	30	2.2	---	0.07
SAB P487	"	---	29.9	0.59	--	4.43	13	0.013	2	0.3	---	2.4	---	0.06
SAB P488	"	---	30.8	0.70	--	4.16	17	0.010	4	0.5	---	1.6	---	0.04
SAB P489	"	0.3	29.8	0.78	--	4.42	13	0.013	2	0.4	35	1.7	---	0.04
SAB P490	"	---	29.2	0.51	--	5.22	11	0.009	17	0.5	---	2.2	---	0.09
SAB P491	"	0.2	31.6	0.63	--	3.53	18	0.011	4	0.4	50	2.4	---	0.03
SAB P492	"	---	29.9	0.58	--	5.02	13	0.008	3	0.5	---	3.2	---	0.09
	Sirat Plateau													
SAB 230	Basalt	1.9	14.2	10.8	6	2.97	7	0.195	210	21	150	48	150	5.0
SAB 493	"	1.7	18.9	11.2	9	1.87	8	0.169	870	27	310	64	---	3.3
SAB 494	"	2.3	13.0	11.7	4	4.31	5	0.166	10	13	100	33	250	6.2
	Jabal at Turf													
SAB 793	Xenolith	0.1	1.35	7.0	46	0.06	0.6	0.125	4700	7.5	40	128	---	0.14
SAB 794	"	0.1	1.78	7.1	43	0.07	0.7	0.126	6100	8.7	40	122	---	0.29
	Jabal Haylah													
SAB 795	Xenolith	0.5	7.62	5.8	16	0.67	15	0.135	2770	50	---	42	175	0.59
SAB 796	"	0.5	6.46	9.0	19	0.81	12	0.177	6100	59	230	64	390	1.5
SAB 797	"	0.6	6.51	8.5	20	0.67	14	0.173	3520	61	300	60	---	0.62
	Pyroxene													
SAB 0794	Separate	0.2	3.80	5.6	33	0.10	1	0.124	9830	20	110	63	---	0.07
SAB C793	"	0.4	4.30	3.1	21	0.77	22	0.084	9170	64	260	30	---	0.40
SAB C797	"	0.6	6.07	4.2	16	1.11	19	0.111	14200	44	260	36	---	0.48
SAB C246	"	1.6	10.0	6.4	14	0.89	19	0.138	1070	61	480	40	---	2.1
CP 53	" Alaska	1.3	10.6	7.6	17	1.47	16	0.149	70	48	350	52	---	1.6
CP AHR	" Alaska	1.8	10.0	8.1	14	1.69	17	0.157	15	51	360	49	---	2.2
CP SR	" Oregon	1.5	4.95	2.2	19	0.35	23	0.118	8530	87	390	40	---	1.4

Table 7. Continued.

Sample #	Th (ppm)	Ta (ppm)	Ba (ppm)	Cs (ppm)	Ir (ppb)	Ni (ppb)	Au (ppb)	La (ppm)	Ce (ppm)	Sm (ppm)	Eu (ppm)	Tb (ppm)	Dy (ppm)	Yb (ppm)	Lu (ppm)
SAB P486	--	<0.01	---	0.06	--	---	---	1.2	2.7	0.35	6.72	0.06	---	0.2	0.03
SAB P487	0.05	0.05	---	0.05	--	---	---	1.8	2.7	0.35	7.52	0.05	---	0.1	0.02
SAB P488	0.02	<0.01	---	0.06	--	---	---	1.0	1.9	0.29	4.53	0.05	---	0.2	0.02
SAB P489	0.07	<0.02	---	0.06	--	---	---	1.7	2.9	0.39	8.47	0.07	---	0.2	0.03
SAB P490	0.04	0.02	---	0.34	--	---	---	3.2	5.5	0.78	7.23	0.14	---	0.4	0.06
SAB P491	0.03	--	---	0.16	--	---	---	0.7	1.4	0.20	5.40	0.04	---	0.1	0.02
SAB P492	0.10	--	---	0.05	--	---	---	1.5	2.8	0.36	8.03	0.06	---	0.3	0.03
SAB 230	0.40	1.2	110	0.08	--	---	---	11.5	26.9	5.6	2.09	0.79	3.2	2.1	0.31
SAB 493	1.1	0.53	100	0.05	--	---	---	9.1	21.5	3.8	1.62	0.77	3.3	1.3	0.27
SAB 494	1.4	2.6	370	0.13	--	---	---	23.7	49.0	6.3	2.40	0.96	4.5	2.2	0.37
SAB 793	0.40	--	---	0.21	--	---	---	0.5	(1.8)	0.10	0.06	0.02	0.4	0.01	0.01
SAB 794	0.40	0.21	---	0.13	--	---	---	0.8	(1.7)	0.16	0.08	0.02	---	0.1	0.02
SAB 795	0.22	0.14	---	0.36	--	---	---	1.1	3.3	1.4	0.54	0.25	1.6	0.6	0.10
SAB 796	0.41	0.32	---	0.15	--	---	---	1.4	5.6	1.6	0.63	0.26	1.3	0.6	0.13
SAB 797	0.93	0.20	---	0.23	--	---	---	1.4	4.5	1.9	0.68	0.34	1.6	0.5	0.11
SAB 0794	--	<0.02	(15)	0.32	3	250	5	0.2	----	0.12	0.04	0.03	0.2	0.2	0.04
SAB C793	--	0.18	---	2.0	6	150	100	1.6	----	1.3	0.50	0.22	1.5	1.0	0.14
SAB C797	--	<0.04	40	8.0	2	160	10	1.3	----	1.3	0.50	0.29	---	1.3	0.20
SAB C246	0.18	0.13	(20)	0.65	6	20	5	2.2	----	3.2	1.20	0.73	4.9	3.4	0.49
CP 53	0.02	0.09	110	10.3	3	50	25	2.5	7.4	2.8	1.04	0.64	3.5	2.5	0.37
CP AHR	0.19	0.12	---	3.2	5	15	20	2.4	7.8	3.2	1.30	0.81	4.5	3.4	0.53
CP SR	--	<0.04	30	0.20	4	70	30	1.9	----	2.4	0.92	0.46	3.0	2.2	0.32

Table 7. Continued.

Sample #	Sample Description	TiO_2 (%)	Al_2O_3 (%)	FeO* (%)	MgO (%)	Na_2O (%)	CaO (%)	MnO (%)	Cr_2O_3 (ppm)	Sc (ppm)	V (ppm)	Co (ppm)	Zr (ppm)	Hf (ppm)
CP NId	Chromium Pyroxenite California	<0.1	0.80	5.7	16	0.69	23	0.087	12300	91	85	25	---	0.04
"Rhyolite"	Oregon Volcanic Ash	1.0	16.1	5.2	6	3.20	4	0.127	40	15	100	12	290	6.8
	Picture Gorge													
6A	Basalt	---	--	10.6	--	1.64	--	---	110	38	---	35	---	3.3
6B	"	---	--	10.1	--	1.56	--	---	95	37	---	33	---	2.8
7A	"	---	--	10.9	--	1.76	--	---	115	45	---	36	210	2.8
7B	"	---	--	12.2	--	1.73	--	---	126	47	---	40	230	3.1
9A	"	---	--	10.7	--	1.67	--	---	40	37	---	36	154	3.0
9B	"	---	--	11.2	--	1.76	--	---	44	39	---	38	254	3.5
12A	"	---	--	10.7	--	1.55	--	---	214	43	---	38	---	2.2
12B	"	---	--	12.1	--	1.59	--	---	215	44	---	39	---	2.3
16A	"	---	--	12.1	--	1.69	--	---	236	49	---	44	220	2.3
16B	"	---	--	11.7	--	1.67	--	---	220	47	---	43	---	2.9

Table 7. Continued.

Sample #	Th (ppm)	Ta (ppm)	Ba (ppm)	Cs (ppm)	Ir (ppb)	Ni (ppb)	Au (ppb)	La (ppm)	Ce (ppm)	Sm (ppm)	Eu (ppm)	Tb (ppm)	Dy (ppm)	Yb (ppm)	Lu (ppm)
CP NId	---	<0.06	70	2.8	8	150	60	0.2	--	0.17	0.08	0.05	0.4	0.2	0.03
Rhyolite	2.8	1.1	670	0.95	--	--	--	24.2	45.4	5.73	1.58	0.86	4.6	1.8	0.23
6A	1.1	0.6	---	0.36	--	--	--	12.5	25.1	4.15	1.45	0.77	---	2.6	0.36
6B	1.1	0.6	---	0.37	--	--	--	13.3	23.0	3.77	1.35	0.82	---	2.4	0.34
7A	0.9	0.6	---	0.31	--	--	--	9.2	19.9	4.02	1.44	0.80	---	3.0	0.44
7B	1.0	0.5	---	0.21	--	--	--	9.3	22.6	3.74	1.62	0.94	---	2.7	0.40
9A	1.7	0.7	---	0.77	--	--	--	17.3	27.0	4.35	1.54	0.80	---	1.9	0.30
9B	1.7	0.6	---	0.53	--	--	--	15.7	29.4	4.26	1.61	0.85	---	3.3	0.45
12A	0.4	0.4	---	0.21	--	--	--	8.6	17.6	3.32	1.42	0.74	---	2.8	0.39
12B	0.4	0.4	---	0.22	--	--	--	8.8	19.9	3.55	1.47	0.70	---	2.7	0.44
16A	0.5	0.5	---	0.14	--	--	--	7.0	18.0	3.49	1.60	0.79	---	2.5	0.40
16B	0.5	0.5	---	0.16	--	--	--	6.4	16.3	3.30	1.53	0.79	---	3.3	0.44

[a] Estimated errors for the elements are: Al_2O_3, Na_2O, MnO, FeO, Co, Sc, ~± 1-3%; Cr_2O_3, TiO_2, MgO, REE, ~± 5-10%; CaO, Rb, Cs, Hf, Th, ~ ±10-20%; Ni, Ta, Zr, ~ ± 20-50%. Standards and duplicate BCR-1 samples were activated with all samples. Abundances of Zr and Th were determined using the concentration in GSP-1 as the standard.

* All Fe reported as FeO.

magnetite in the last stages of fractional crystallization.

Ilmenite is usually found in the later stage of the magmatic sequence and will therefore occur in gabbroic rocks. Titanium may also be seen in some early formed pyroxenes. Titanium can either occur in the trivalent or quadrivalent state in the geochemistry. The quadrivalent state is found in ilmenite or it is captured by the Al site in Al minerals. The trivalent state is the most common in the remaining minerals.

Titanium varied in the gabbros and the mineral separates studied in this work. Titanium was found only in the plagioclase minerals when the associated gabbros rock had a corresponding high (>1.5%) TiO_2 content. There was no similar relationship noted between the pyroxenes and the associated xenoliths. The Jabal at Turf xenoliths had a very low TiO_2 content.

Titanium shows many correlations in both the gabbros and xenoliths. In the gabbros positive correlations were found with Fe, Mn, Zr, Hf, and the REE, and negative correlations, with Ca. In the xenoliths, positive correlations were obtained with Al, Na, Ca, Sc, V, and the REE, and negative ones, with Mg and Co.

Aluminum: Aluminum is one of the most abundant elements in igneous rocks. Trivalent Al is intermediate between the radius for tetrahedral and octahedral coordination. In octahedral coordination Al will act as a pure cation, while in the four coordination it will act

as the central atom of the anions. The ability to change coordination is the most important part of Al geochemistry. This coordination may be controlled by the temperature and acidity of the magma from which the Al is crystallized. Aluminum content increases in the melt until the feldspars start to crystallize and most of the Al is removed in these minerals. After these minerals have crystallized the Al content again rises in the residual magma until the final stages of crystallization.

The most important Al minerals are the feldspars which may contain as much as 60% by weight of the average igneous rocks. Aluminum is usually found in combination with silicon but can be found associated with other elements in some minerals. The richest Al containing rocks are plutonic rocks of which gabbros are an important group. Goldschmidt (1958) states that the average gabbro contains about 12 to 20% Al_2O_3, which is similar to the gabbros analyzed in this study. Aluminum abundances are very high in plagioclase feldspars with an average of about 30% Al_2O_3, which was again obtained for the plagioclase separates listed in Table 7. Magnesium olivine rocks and pyroxenes are believed to have Al abundances only in the ppm range. This was not borne out in my investigation since the range for the pyroxene separates were 1 to 10% Al_2O_3 (Table 7).

The xenoliths that were analyzed can be divided into two groups

by the Al content as suggested by Harris et al. (1967). These two groups may be divided by Al_2O_3 content of 2% or less and those of greater than 3% Al_2O_3. These two groups may again be characterized by their CaO abundance. The Jabal at Turf xenoliths are associated with the first (<2% Al_2O_3) group and the Jabal Haylah (JH) xenoliths are from the later group. The members of the low Ca-Al abundance group are virtually lherzolite, which may be partially depleted or residual mantle material. The members of the high Ca-Al group are eclogite or websterite and probably represent mantle material with no changes (Harris et al., 1967).

Aluminum in the gabbros correlates well with Mg, Sc and Co and inversely with Mn. In the xenoliths I found many unexpected correlations; e.g., Al in xenoliths correlates positively with Ti, Na, Ca, Sc, V, and the REE and negatively with Mg and Co.

Iron and Cobalt: Iron is among the earliest elements to crystallize during the main differentiation process. It is not involved in the first stage of crystallization due to the presence of Mg. Iron is a very versatile element and enters most minerals. Because of the similarity of the ionic radii of divalent Fe and Co, these two elements follow each other very closely with Co as a trace element in the ferrous minerals. Cobalt may even follow trivalent Fe. The early Fe and Mg crystallization involves formation of olivine. Olivine composition varies from Mg rich to Fe rich as the differentiation progresses.

The Co is found much more prominently in the Fe rich than in Mg rich olivines. Iron is also found in the middle sequence of crystallization in pyroxenes and plagioclase as well as other minerals. Iron is found in all minerals in either trace or minor amounts. The amount of Fe in any mineral depends on the oxidation state of the Fe in the residual magma at that particular time of crystallization. Cobalt will follow Fe in most of the minerals, but the ratio of Co/Fe will decrease as the chemical differentiation proceeds, due mainly to the decrease in Co content.

The Fe content for the gabbros of this work varied from 5 to 12% FeO as was expected for the whole sequence of crystallization. The Fe content of the plagioclase minerals was much less than the pyroxenes. Iron must replace Ca in the plagioclase whereas in the pyroxenes Fe may simply replace the Mg. The Fe content in the xenoliths was fairly constant for the entire group.

The Co content was fairly constant for all of the samples with the exception of the plagioclase separates and the Jabal at Turf xenoliths. The average Co content for most of the gabbro samples was ~50 ppm which was expected since Co should remain fairly constant until the very end of the crystallization sequence. In the plagioclase the Co contents ranged tightly from 1 or 2 ppm. The one set of xenoliths has a very high Co content of 125 ppm.

Iron shows similar positive correlations in both the gabbros

and the xenoliths with Mg, Mn and V in both rock types and with Ti in the gabbros and Ta in the xenoliths. Cobalt on the other hand shows quite varied correlations between the two samples. The gabbros show positive Co correlations with Al and Mg and a negative Co correlation with Na. Cobalt in the xenoliths shows positive correlations with Mg and REE and negative correlations with Al, Ti, Na, Sc, and Ca. This indicates that Co associates as a trace element with other minerals rather than Fe containing minerals.

Nickel: The geochemistry of Ni will be similar to Co but due to the difference in ionic radii between Co and Ni, Ni is captured more by Mg than the Fe minerals. It is observed that the Co/Ni ratio is higher in the later Fe minerals than in the early Mg minerals because Ni is removed from the melt in the first part of the crystallization.

In this study Ni was only determined in the pyroxene samples. The Ni abundances were low in the pyroxene separates from the basalt rocks but were about five times as large in the xenoliths. It therefore seems that most of the Ni in the earth remains below the crust.

Manganese: Manganese is the most abundant minor element in the magmatic process. Due to the similar ionic radius of the divalent state and the multiple valency states, Mn may replace Fe, Mg or Ca in various minerals. Manganese may also be associated with Sc in some minor minerals. Manganese is also found in the early Mg minerals of olivines and pyroxenes and in the later Fe minerals of

magnetite and ilminite. Some Mn is also found in the plagioclase feldspars where it replaces Ca. The total divalent ion content is believed to decrease as crystallization increases, but the divalent Mn content increases until the latest crystallization stages.

A distinctive feature of Mn geochemistry is the increase in the Mn/Mg ratio which increases from 1:100 to 1:1 as the crystallization process goes to completion (Goldschmidt, 1958). This ratio can then be used to determine the approximate "stage" of evolution of the rocks. According to this ratio the gabbros of this work were at the point of 30 to 40% crystallization.

Manganese is thought to be in the highest abundance in the gabbroic rocks and maybe in basalts. The Mn abundance in granites is very low, and therefore, Mn should be removed in the last minerals to crystallize before granites, the plagioclase minerals. This is not shown in the analyses of this work because the Mn content in the plagioclase separates is about ten times lower than in the gabbros. The pyroxene mineral separates, the gabbros, and the xenoliths all appear to have about equal Mn contents. If the ratio of Mn/Mg is expected to be a sensitive indicator, it appears that the plagioclase separates must be one of the last minerals to crystallize since the Mg content is too low to be detected.

Manganese shows positive correlations with Fe and the REE in both series of rocks, with Ti in the gabbros, with Sc, V and Na in the

xenoliths, and Mn shows a negative correlation with Al in the gabbros.

Magnesium: Magnesium forms heavy minerals and these will be concentrated in the lower crust at zones by settling out from the liquid magma. Most Mg minerals are also high temperature minerals and will solidify early. Magnesium is found mainly in peridotites, pyroxenites and olivines with concentrations that range from 50% MgO down to around 0.1% MgO in the rocks. First fractions of pyroxenes and olivines will be enriched in the magnesium component and later fractions will contain ferrous components. Trace amounts of Ni, Co, Zn, Mn, Sc, In and Hf may also replace the Mg or Fe in these minerals but these trace elements will not upset the distribution of Mg relative to Fe in the magmas. Scandium will be found more readily in the pyroxenes than in the olivine or peridotites.

The Mg content in the samples varies considerably depending on the minerals present. The plagioclase minerals have MgO content below the limit of detection while the pyroxenes have a content of 15 to 30%. The gabbros have intermediate MgO contents of 3 to 11%. The xenoliths are the interesting group because the MgO content is inversely proportional to the $CaO\text{-}Al_2O_3$ content. In the Jabal at Turf group with low $CaO\text{-}Al_2O_3$ content about 45% MgO was found, while in the Jabal Haylah xenoliths series with higher $CaO\text{-}Al_2O_3$ contents about 20% MgO was found.

The Mg correlations were almost a reversal of most other

correlations in that the xenoliths show many negative correlations. The only positive Mg correlation for the xenoliths was with Co while the negative ones were with Na, Ca, Sc, V, Ti, Al and the REE. In the gabbros, a positive Mg correlation was found with Co, Al and Fe and a negative correlation with Na.

Calcium: Calcium minerals are formed during the transition between the early and middle stages of the sequence of fractional crystallization. The Ca minerals have relatively low densities and tend to rise in the magma pool. Calcium forms pyroxenes, plagioclase and some other Ca minerals found exclusively in mafic gabbros and basalts that are rich in alkali metals. Sodium, having a slightly smaller radius than Ca will be admitted into Ca minerals and increasingly more in the late crystallizations. Calcium plagioclase, being a higher temperature crystal than sodic plagioclase, will crystallize out of the magma first and deplete the Ca content in the magma.

Manganese will also replace Ca in the minerals due to a smaller radius. The trivalent ions of the REE will readily enter Ca plagioclase minerals (Figure 6) and can show a depletion in the Tb to Lu section of the REE series. The depletion of La-Tb of the REE is shown in the pyroxene separates (Figure 8).

The CaO content for all of the samples except for the xenoliths show approximately the same concentration. The CaO contents in the xenoliths again distinguish two separate xenolith groups as discussed

in the Al section. The Jabal at Turf xenoliths have CaO concentrations of less than 1% which represents the lherzolite type, a possible representative of depleted mantle material. The other set of xenoliths, Jabal Haylah, represent the high Ca-Al group labeled eclogite or websterite rocks, which may be the pure mantle material (Harris et al., 1967).

For the gabbros, only negative Ca correlations were obtained with Ti, Na, Ta and the REE. The Ca correlations for the xenoliths gave positive ones for Sc, V, REE, Ti, Al and Na and negative ones for Co and Mg.

Sodium: The geochemistry of Na is dominated by its ionic radius which closely resembles that of Ca. Sodium will replace Ca mainly in the later crystals rather than the early Ca crystals. Sodium will not enter many minerals as a main ion but will usually replace Ca or some other similar element. The alkali elements, Na and K, will not replace each other since there is a rather large difference in their ionic radii.

The feldspars and pyroxenes should contain Na/Ca in the ratio of 1:10 (Goldschmidt, 1958; Manson, 1965). This ratio is about the average value obtained for the samples of this work. The plagioclase gave a ratio of 1:4, while the pyroxenes gave an average ratio of 1:15. Sodium remains in the residual solutions and is distributed to a large extent by hydrothermal processes in the last fractions. This

hydrothermal action or alteration may also present a problem of alteration of the xenoliths by replacing some Ca in the rocks with the Na from the magma. This alteration may be difficult to prove one way or another.

In this study Na was found to be concentrated in the plagioclase separates by a factor of two over the gabbros and pyroxenes. The xenoliths were both very low in Na with the Jabal at Turf group a factor of ten lower than the Jabal Haylah group.

The Na correlations with Ca, Cr, Co and Mg were all negative for the gabbros. The xenoliths again gave a large number of positive correlation. Positive Na correlations were obtained with Ca, Mn, Sc, V, Ti, Al and the REE. The negative Na correlations for the xenoliths were again Co and Mg.

Potassium, Rubidium and Cesium: These alkali metals are characteristic of residual stages of magma evolution owing to their large ionic radii. These three elements are all closely related in their geochemistry and the major differences in behavior are their total abundances in the upper crust. Rubidium will enter K minerals, feldspars, much more easily than Cs will, but in most minerals Rb and Cs will concentrate together. Potassium will either be concentrated in feldspars or biotite, while the Rb and Cs are mainly concentrated in the later granophyres or in the hydrothermal minerals.

Cesium was the only element of these three alkali elements that

was determined during the INAA procedure and its abundance was low (<1 ppm) except in the pyroxenes where Cs ranged from 1 to 10 ppm. Using the RNAA procedure, it was found that K was highly concentrated in the gabbros (1100 ppm) while the mineral separates had about 700 ppm. The Rb was concentrated in the pyroxenes as much as in the gabbros and was low in the other samples. The Cs abundance followed that of Rb, and the Cs abundances were about a factor of 10 lower than Rb abundances.

Chromium: Chromium is one of the first elements to be crystallized during the magmatic process as chromite or as chromium-spinels. Chromium is also found in high amounts in the olivines and pyroxenes. Chromite is present in the early gabbroic melts and crystallizes out in the Mg rich rocks. Chromium is removed from the residual liquid in the first stages and is therefore found only in small quantities in the Fe minerals and the plagioclase minerals.

The Cr content of the gabbros varies considerably as is expected because of the early crystallization of Cr minerals. This variety of Cr concentrations is probably due to the inclusion of chromite in the crystallized gabbros. Both the lherzolite and websterite xenoliths had exceedingly high contents ranging from 2800-6100 ppm Cr_2O_3. On the other extreme, plagioclase separates from the gabbro rocks contained only 2 to 17 ppm Cr_2O_3. The pyroxenes showed great variations depending on the parent rocks. Both the

orthopyroxenes and clinopyroxenes from the xenoliths as expected had 0.9 to 1.4% Cr_2O_3, and the one pyroxene from California, U.S.A. had a large Cr content since it was a chromium pyroxenite. The two pyroxene crystals from Alaska, U.S.A. show exceedingly low contents of 17 and 50 ppm Cr_2O_3.

Due to the possible incorporation of chromite or chrome-spinels into rocks, no correlations were found with any of the other elements. Since Cr is one of the first elements to crystallize it may associate with many elements but none consistently.

Scandium: Many authors disagree on the chemical behavior of Sc in nature; some suggest that Sc follows the REE and others indicate that it will follow both Fe and Mg (Norman and Haskins, 1967; Goldschmidt, 1958). If Sc follows the REE then it would be expected to be concentrated late in the crystallization process. If it follows Fe and Mg, it will be concentrated in the olivines and pyroxenes. Goldschmidt (1958) states that Sc will be concentrated in the early ferromagnesium rocks. This study supports his hypothesis since Sc was concentrated twice as much in the pyroxenes compared to the whole gabbro rocks and ten times as much as in the plagioclase separates. The Sc contents in websterite xenoliths were about seven times greater than the Sc contents in lherzolite xenoliths. A similar concentration effect was observed for V in these two xenolith sets. The Sc content in the gabbros is about what is expected with an

average of 30 ppm.

Scandium correlates positively with Al in both groups. In the xenoliths, positive correlations were found with V, Ti, Na, Ca, Mn and the REE, and negative correlations, with Co and Mg. The positive correlations between Sc and V suggests that both are concentrated in the clinopyroxene rather than olivine and orthopyroxene.

Vanadium: Vanadium is believed to crystallize out during the middle stages of the crystallization process. Due to the ionic radius of the trivalent state, V follows Fe or Cr in its geochemistry. The gabbroic and basaltic rocks formed in the crystallization process may have from 150 to 300 ppm of V present as was also found in the samples of this study.

Vanadium in nature is found mainly in either magnetite or chromite depending on which element, Fe or Cr, it is following in that stage of crystallization. The main V concentration is found in magnetite and may either come from the magma itself or be concentrated in the magnetite due to hydrothermal leaching from other rocks and deposited in the magnetite. The V content found in pyroxenes rarely exceeds 500 ppm.

The V contents in all of the samples except the plagioclase separates are rather similar and show little variation due to the differences in magma origins. Vanadium appears not to be a very useful element in determining the rock type or the stage of evolution.

In the gabbros the only positive V correlation was one with Fe. The xenoliths contained many unexpected correlations. Positive correlations with Ti, Al, Fe, Na, Ca, Mn, Sc and the REE and negative correlations with Co and Mg were found. See the Sc discussion above.

Barium and Strontium: The geochemistries of Ba and Sr, both LIL (large ion lithophile) elements, are strongly influenced by their ionic radii. Both have radii that are considerably larger than Fe and Mg and will be found in trace quantities in the respective minerals. The radii are very similar to K; therefore, Ba and Sr are found in the early K minerals in the sequence of crystallizations. Due to the large sizes both elements are concentrated in the residual magma and will show up mainly in the K feldspars and plagioclase. These elements are sparsely abundant in the pyroxenes with Sr a little more abundant than Ba. The Sr content in the whole rock is much more dependent on the plagioclase content than is Ba. Strontium is much more concentrated in the gabbros than Ba.

Barium and Sr were obtained mainly in the radiochemical scheme and showed the differences as stated above. The contents of these elements in the various minerals and whole rocks is shown in Table 6. In the pyroxenes, the Ba contents were below the detection limit and in the plagioclase, 880 ppm. The same was found for Sr, 24 ppm vs. 1700 ppm in these minerals respectfully.

Rare Earth Elements (REE): Half of the REE were analyzed via

the INAA procedure and all 14 REE were analyzed by the RNAA procedure. The elements obtained by INAA were La, Ce, Sm, Eu, Tb, Yb, Lu and sometimes Dy.

The REE act similarly as a group in nature due mainly to the similar ionic radii of the trivalent state. The radii for the hexacoordinated trivalent REE ion range from 1.13 Å for La down to 0.94 Å for Lu (Whittaker and Muntus, 1970). The trivalent state is the most common in the REE geochemistry but in some minerals, plagioclase, divalent Eu may also be present.

The REE pattern in a chillzone may represent a pattern close to that in the original melt. The REE are mainly concentrated in the later residual liquid during the magmatic sequence and then they may replace the divalent Ca in the very last minerals. The remaining REE will be concentrated in the granitic rocks. The REE are one of the most fascinating groups to study due to the chemical regularity of the group.

The most common method for illustrating the REE results is to graph the REE abundances normalized to the average of ordinary chondritic meteorities as shown in Figures 2 to 9. The normalized abundances are plotted against the ionic radii (Whittaker and Muntus, 1970). A separate series of curves is shown for each of the sample groups to illustrate the relative trends. When these curves are compared among themselves and with other petrographic rock types

(Coles, 1972) it is seen that each rock type is represented by uniquely shaped curve.

The REE curves for the Jabal at Turf (JT) gabbros show a smooth curve (Figure 2) with a positive Eu anomaly which is about two times larger than the expected Eu value obtained by extrapolation between Sm and Gd, the adjacent REE. The Eu enrichment is probably due to the high content (~45%) of plagioclase in the whole rock. One of the gabbros (SAB 491) shows an overall REE depletion of two to four from the remaining gabbros in the series. The possible chillzone sample (SAB 215) shows a REE pattern completely different from the gabbros in that it shows an enrichment of the light REE and no Eu anomaly. This pattern could possibly represent the REE content in the original undifferentiated magma.

The REE curves for the Jabal Shayi (Figure 3) are not as uniform and the JT REE curves and the JS patterns are all similar. The JS chillzone material does not show the different REE pattern as seen in SAB 215. These JS gabbros do show a significant depletion in the heavier REE relative to the light REE.

The xenoliths present REE curves that show interesting features (Figure 4). The two Jabal at Turf lherzolite xenoliths show REE patterns very similar to that obtained for most plagioclase minerals only with a smaller Eu enrichment. The JT xenoliths have a light REE enrichment of about ten times over the heavy REE. However because

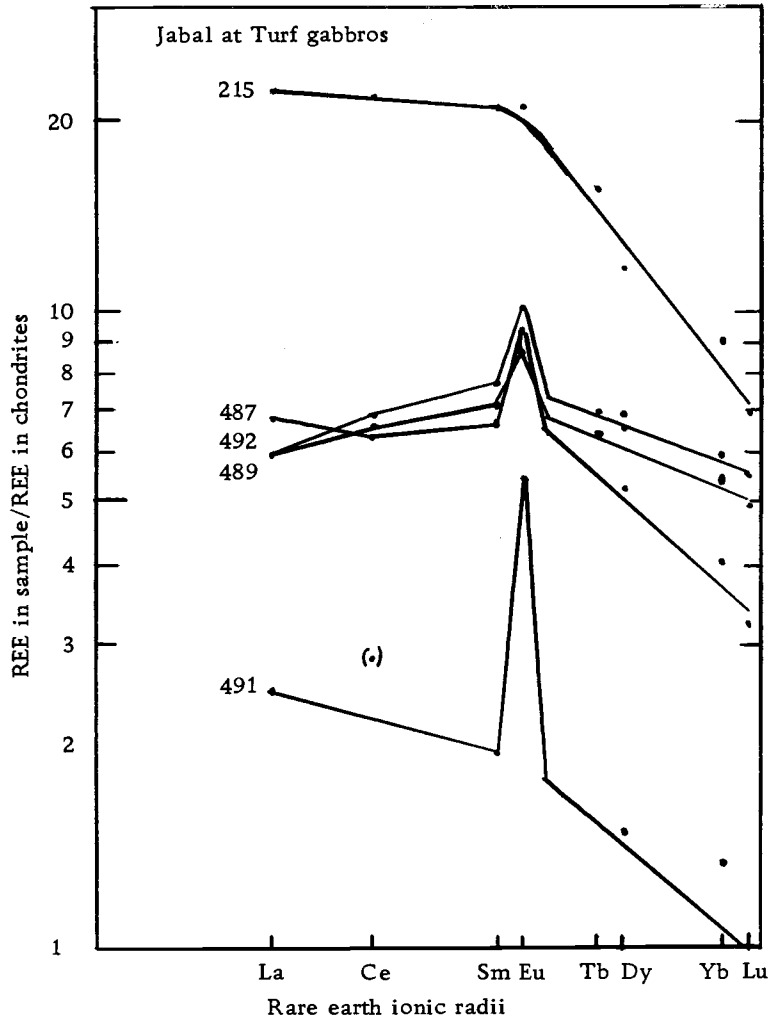

Figure 2. JT gabbros; 215 is chillzone rock; 491 is a high plagioclase gabbro.

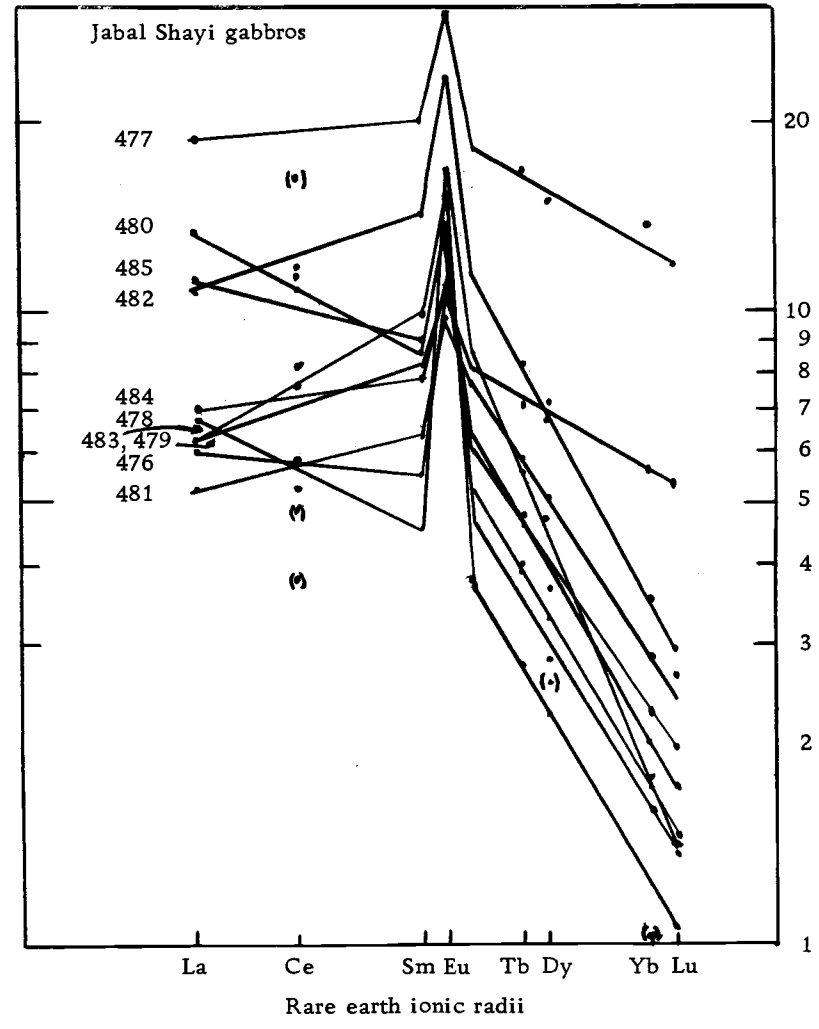

Figure 3. JS gabbros; 483 and 485 may be chillzone rocks; remaining gabbros are layered gabbros showing no differentiation with height.

these samples are very low in Al_2O_3 (~1%), they have little if any plagioclase. The Jabal Haylah (JH) websterite xenoliths show a REE pattern that is either depleted in both the extreme light and heavy REE or enriched in the central REE region of Sm and Eu. This pattern cannot be explained simply by mixing of common minerals.

The two series of basalts that were analyzed gave similar REE patterns (Figure 5) even though they are from two completely different areas. There is a gentle positive slope from the light to the heavy REE, with a difference of about seven times between the two ends. Some of the Picture Gorge basalts show a slight positive Eu anomaly. The one volcanic ash sample, Rhy, shows a similar slope as the basalts with a slight negative Eu anomaly.

All of the plagioclase separates from the Miocene and Precambrian gabbroic rocks show a similar REE pattern (Figures 6 and 7). Both the Jabal at Turf and Jabal Shayi plagioclase separates show a factor of two difference between the light and heavy REE, with a positive Eu anomaly of about 40 to 50 times the extrapolated value. This Eu enrichment is attributed to the accommodation of divalent Eu ion into the plagioclase lattice.

The clinopyroxene REE curves (Figure 8) are all similar in that the light REE are depleted relative to the heavy REE by a factor of two. One sample, CP-NId, has the same approximate curve but is lower in abundances by a factor of ten. This sample is a chromium

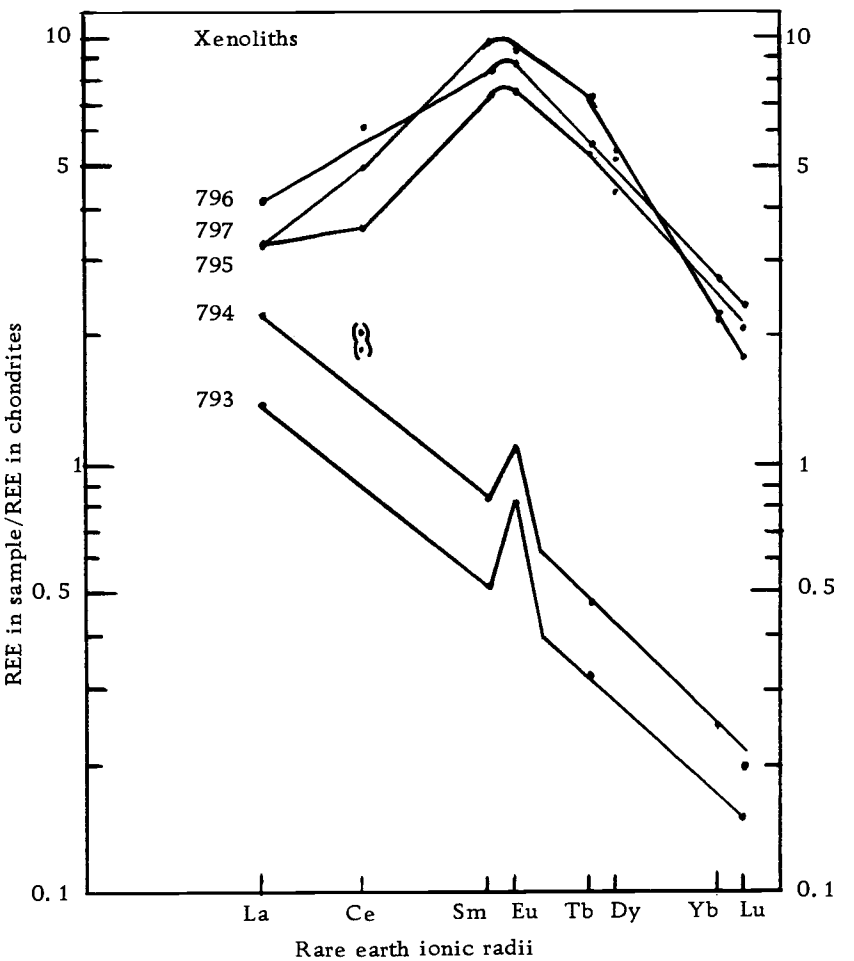

Figure 4. Xenoliths; samples 793 and 794 are lherzolites from the Jabal at Turf area; samples 795, 796 and 797 are websterites from Jabal Haylah samples.

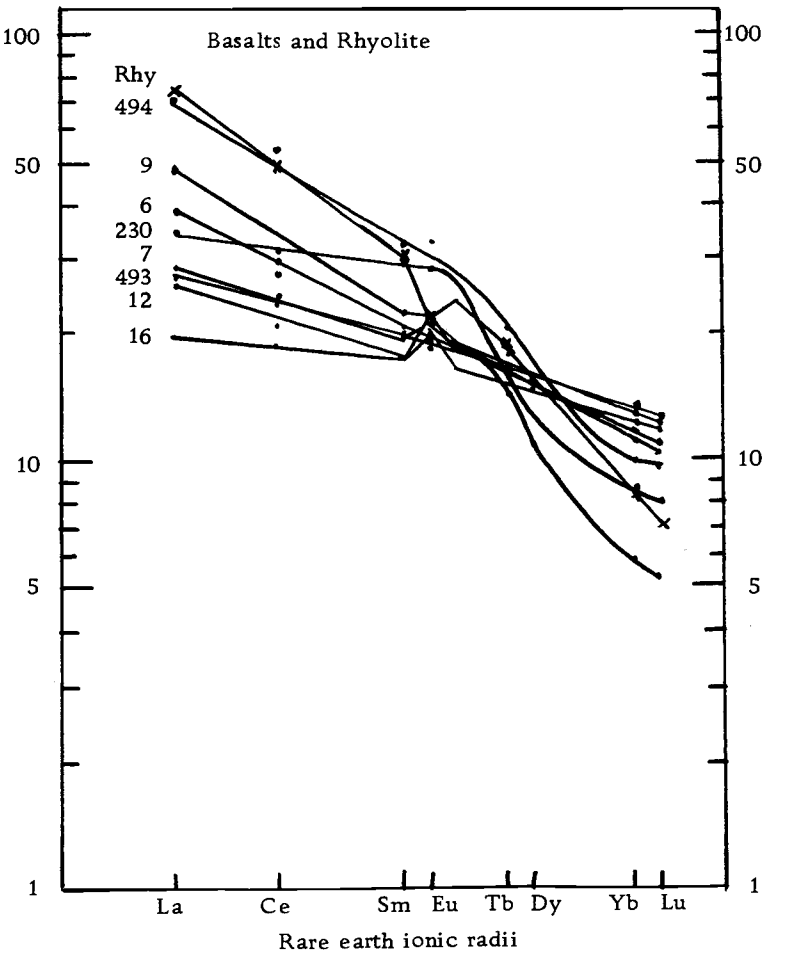

Figure 5. Basalts and rhyolite sample; 6, 7, 9, 12 and 16 are the average of the two splits from each Picture Gorge basalt; 230, 493, and 494 are Sirat Plateau basalts.

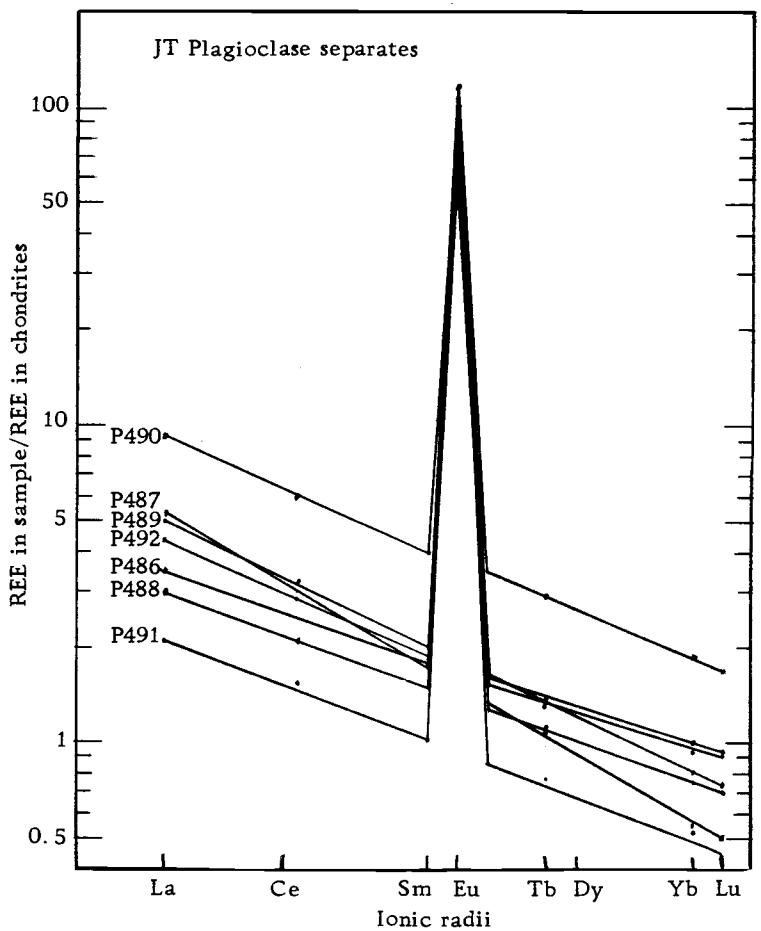

Figure 6. JT plagioclase separates.

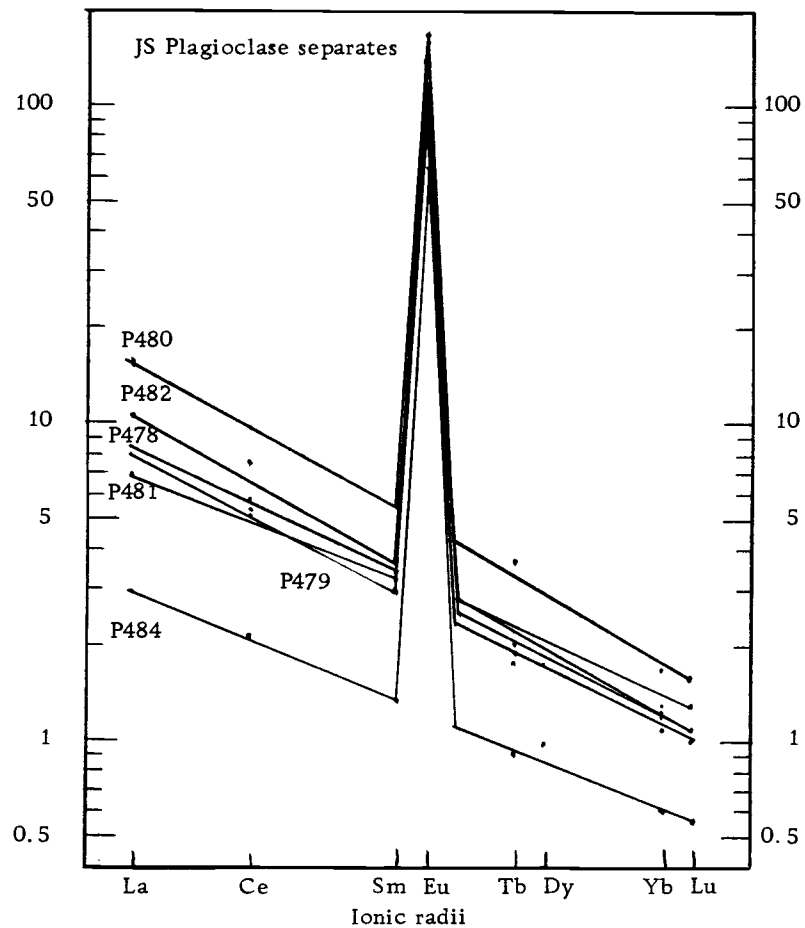

Figure 7. JS plagioclase separates.

pyroxene which probably crystallized from a magma depleted in REE. The orthopyroxene sample shows a curve that is enriched in the heavy REE.

The final REE curves shown in Figure 9 are the ones obtained in the samples that were analyzed by the RNAA procedure. These curves are considered to be more accurately defined because all 14 REE abundances were used to define the curves. These curves tend to support the earlier discussion of REE patterns. Some of the differences found may be attributed to sampling problems, e.g., sampling 0.5g for INAA vs. 0.05g for RNAA and approaching sensitivity limits by INAA for some of the elements. Some of the samples were whole crystals, viz. plagioclase, and pyroxenes, but most were crushed samples. The REE values obtained for BCR-1 in the work via INAA and RNAA techniques both agreed with literature values. I believe that the La abundances obtained by RNAA are the more reliable values due to the much lower sensitivity of the separation procedure.

In the xenoliths there were positive REE correlations with all elements except for Fe. In the gabbros, the REE correlate positively with Mn, Co, Ti, Zr and Hf. There were no negative correlations found for the REE in this study.

Hafnium and Zirconium: These two elements are chemically similar despite the different atomic number and weights. These two

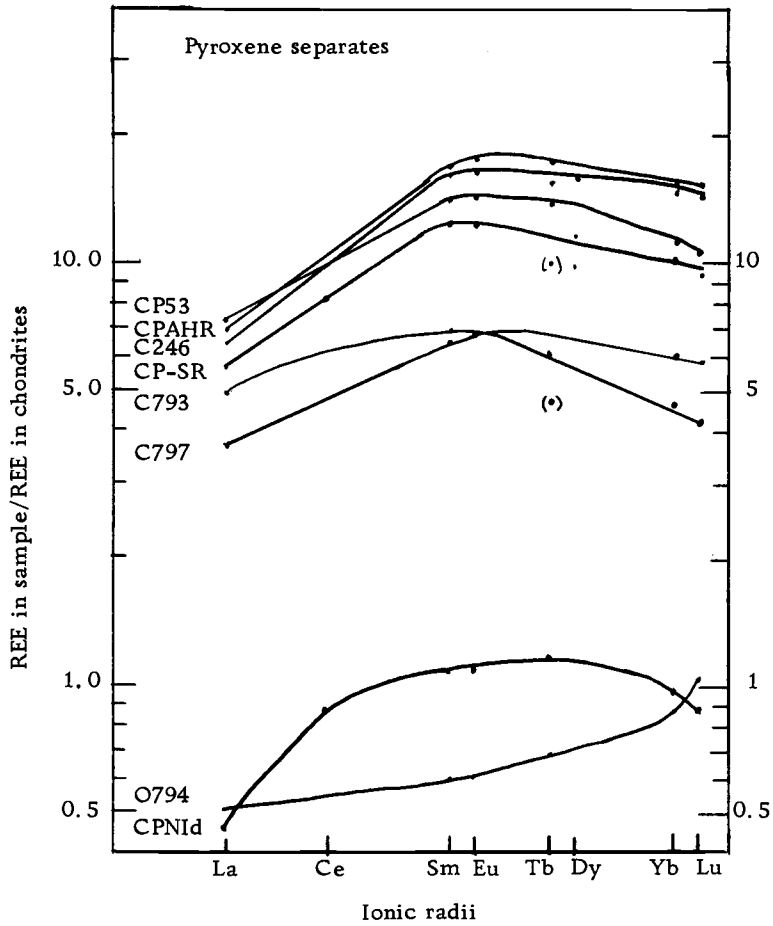

Figure 8. Pyroxene separates.

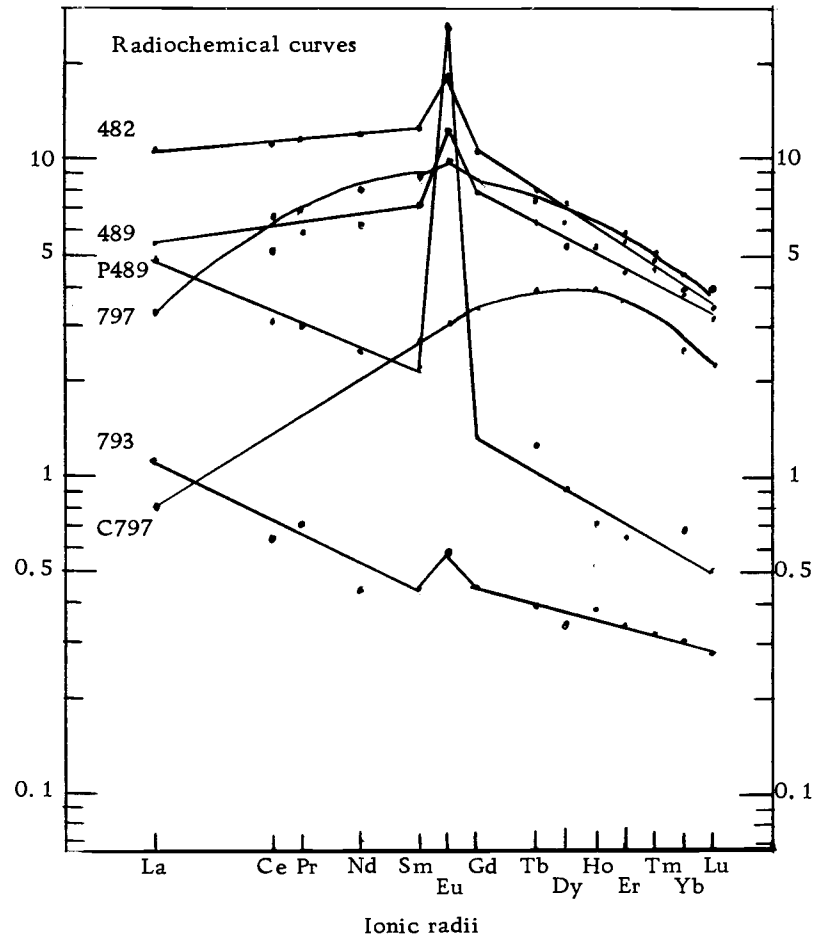

Figure 9. Radiochemical REE curves.

elements are separated by the second transitional series and the lanthanide series; the ionic radii of Hf and Zr are nearly identical.

These two elements are concentrated in residual magmas, expecially in those magmas characterized by large contents of alkali minerals. Zirconium does not enter into any of the common rock-forming minerals, but generally forms its own mineral (zircon) in the later stages. Hafnium is camouflaged in the Zr minerals. The Zr/Hf ratio remains almost constant throughout the differentiation process except in the high Zr minerals. Hafnium and Zr may also enter the pyroxene with as much as 50 ppm present.

Large errors associated with the Zr abundances preclude any serious discussion of Zr. The Hf contents ranged from 0.1 to 2.2 ppm for all of the samples except for the plagioclase separates which have 0.005 to 0.09 ppm with an average of 0.04 ppm.

Zirconium and Hf correlated only with the REE in this study, which could be due to the fact that all of these elements are found in the residual liquid.

Tantalum: Tantalum is found predominently in the last minerals to be crystallized, the plagioclase feldspars. Tantalum follows Nb in its geochemistry and will concentrate in the residual magmatic liquid until it is of high enough concentration to form its own minerals. To a very small extent, Ta may be captured by some Ti minerals. In this work Ta was found predominantly in the JT lherzolite xenoliths

ranging from 0.5 to 2.5 ppm and Ta was very low (<0.2) in the remaining samples. The only correlation of Ta was with Fe and Hf in the gabbros.

Thorium: Thorium is a LIL (large ion lithophile) element and is concentrated in the residual liquids until the later stages of magmatic differentiation. The geochemistry of Th is mainly due to its close ionic radius with that of other elements, Th^{+4} (1.08 Å) and the REE, all LIL elements. Thorium also shows a close relationship with U. Since Th remains in the residual liquid it is found mainly in the granophyres. Thorium may also resemble Zr and Hr as well as the REE in its chemistry. In the last stages of crystallization Th and U will enter the light density minerals and will then be concentrated in the upper part of the crust.

The Th content in the plagioclase separates ranges from 0.02 to 0.10 ppm, while in the whole rock gabbros, both JT and JS, the Th content varies from 0.11 to 0.24 ppm. This indicates that the plagioclase is not the major contributor to the Th content of the whole rocks. Clinopyroxene, with an average Th content of ~0.2 ppm, will contribute the greatest amount to the whole rock gabbro.

IV. DISCUSSION

Gabbros

In the Jabal at Turf gabbro series (20-24 m. y.), four layered samples and the associated chillzone were analyzed. These samples, differing only in the distance from the basal contact, are believed to be from the same magma source. From Figure 2 and Table 7 it is evident one of the gabbro samples SAB 491 (18480 m. above basal contact) is different from the rest of the layered series. Samples SAB 487 (1050 m.) 489 (7300 m.) and 492 (18480 m.) all have similar REE curves, bulk and minor element compositions. The main difference is the plagioclase content of the samples. SAB 491 contains ~60% plagioclase in the whole rock sample and there were ~40% plagioclase in the remaining gabbro samples. This plagioclase content as determined by the Al_2O_3 content also explains the lower REE curves with the greater Eu anomaly for SAB 491 as compared with the others. All of the gabbros exhibit a positive Eu anomaly which is not found in the chillzone sample.

Another possibility for the difference between SAB 491 and the remaining JT layered gabbros is the amount and composition of any trapped liquid. As long as the parent liquid continues to circulate through the open pores of the crystals, growth of the crystals (adcumulus growth) will continue. Some of the parent liquid may

become trapped in the pores and be foreced to solidify as part of the complete rock (orthocumulus growth) (Paster et al., 1973). This factor of trapped liquid present in the crystal lattice could account for the difference in REE patterns as well as the element contents if SAB 491 contains less trapped liquid than the remaining gabbros.

The sample SAB 215 is the associated chillzone for the Jabal at Turf series. This sample had differences in the bulk and minor elements especially in the Ti, Fe, V and Ca contents. This sample also yielded a distinctively different REE curve (see Figure 2) from the gabbros. This sample shows no Eu anomaly and may represent the original REE content. As expected all gabbro samples have lower REE contents than the chillzone sample.

It is difficult to derive an origin that could supply the determined REE curve. The major element concentration is similar to that of an oceanic basalt with some Ca-minerals replaced by the Fe-minerals to a minor extent. This leads to the possibility of a depletion of pyroxene minerals from original oceanic tholeiitic basalt magma before intrusion into the upper crust. This could present a means of deriving the REE curve of the chillzone sample, SAB 215, by starting with the REE curve for the oceanic basalts as shown by Coles (1972) and then the removal of the pyroxenes. This would then account for the heavy depletion of the Tb-Lu region of the curve. With this idea and some other minor crystal settling the REE curve for SAB 215

can be derived.

The Precambrian Jabal Shayi series of gabbros SAB 476 to SAB 485 are a completely different group of gabbros. They seem to be a common group of samples with no real difference among the sample lot. The absolute REE contents may differ from one sample to the next but the chondritic normalized patterns are all similar. The bulk and minor elements also vary somewhat but there is no specific pattern or trend to the changes. The apparent JS chillzone samples, SAB 485 and SAB 483, do not show any different REE patterns or bulk and trace element contents compared to the JS layered gabbros. These JS observations contrast sharply with the chemical differences observed between the JT chillzone and the associated upper layered gabbros. The data indicates that the SAB 485 and 483 samples are not true chillzone material.

The REE abundances in rocks from most layered series usually differ little from that of the chillzone gabbro. The bulk of the REE remain trapped in residual liquid. The loss of the REE to the various minerals is small compared to the total REE abundances in the magma. Most of the deviations from that of the chilled gabbro may be attributed to the effects of selective acceptance by the minerals and varying degrees of inclusion of interstitial liquids. The deviations can also be minimized by the simultaneous precipitation of minerals that prefer heavy REE (e.g. pyroxenes) and light REE (e.g.

plagioclase). The accumulation of plagioclase feldspars would cause the residual liquid to be significantly depleted in Eu relative to the other REE. This depletion is not seen in any of the samples that I analyzed.

Coleman et al. (1972) suggest the gabbros may have originated from a tholeiitic parent magma. This is suggested by his determination of low potassium values in the gabbros. This belief is supported by the fact that the REE contents in the gabbros analyzed for this study are less than those given by Coles (1972) for the average oceanic tholeiite by factors of two to four. The gabbros also have REE contents that are two to three times lower than the HBA samples analyzed by Coles (1972). The depletion of the REE in the gabbros are probably due to the cumulate nature of crystallizing plagioclase, pyroxenes, and olivines (Coleman et al., 1973).

From the REE patterns shown in Figures 2 and 3 it seems reasonable that the two gabbro series came from a similar type of magma. The REE patterns are similar in both the JT and JS series. Assuming the same magma source for all gabbro layers, individual variations in the absolute REE and other LIL element abundances may be attributed to varying degrees of adcumulus and orthocumulus growth. The steep slope for the heavy REE indicates that the magma from which these gabbros crystallized was considerably depleted in heavy REE. This suggests a garnet bearing source in the mantle for

partial melting to obtain the original magma. A mixture of clinopyroxene with the plagioclase can account generally for the REE pattern shown in the figures for the gabbros. The crystallization of orthopyroxene and olivine will not affect the REE pattern much.

Laul and Schmitt (1972) found two lunar basaltic rake samples, 15643 and 15388, that have normalized REE patterns that resemble the patterns obtained for the gabbros in this study.

In comparing the REE content in the JT and JS gabbros with those determined for the Skaergaard gabbro series by Haskins et al. (1968) and Paster et al. (1973) many differences were found. The values for the upper zone A (UZA) in the Skaergaard series (Haskins et al., 1968) are the only REE abundances that resemble or come close to the contents of the JT or JS gabbros. The values as determined by Paster et al. (1973) are four to eight times the REE contents of the JT samples and most of the JS samples. Some JS samples (SAB 477 and SAB 480) have REE contents that vary from equal to one-third as much. SAB 491 being much lower in total REE content will vary from the Skaergaard series by much greater amounts than the remaining gabbros. It therefore can be concluded that the Skaergaard gabbros contain a higher REE content compared to the Saudi Arabian gabbros. Therefore it would not seem possible that these gabbros from the two different locations are from a similar magmatic origin. The two Saudi Arabian gabbro series show a very

close similarity in the REE content and pattern, while the overall agreement with the Skaergaard Intrusion was not that close.

Xenoliths

The elemental abundances for the xenoliths, as shown in Table 7, indicate there are two distinct groups of xenoliths present. The Jabal at Turf xenoliths are from the group called lherzolites which are noted for their high (5-10) $MgO/\Sigma FeO$ ratio. Also common to these samples are the very low Al_2O_3 and CaO concentrations. The JT xenoliths have REE patterns that resemble the plagioclase separates (Figures 6 and 7). The high MgO content is attributed to a high olivine content in the sample. As pointed out previously, the low Al_2O_3 content rules out significant indigenous plagioclase or contamination. The extremely large Cr_2O_3 content may also be due to the entrappment of chromium spinels which are common in the lherzolites (Kuno, 1969). It is possible that these lherzolites (olivine and opx) could represent the residue of the partial melting of an olivine, orthopyroxene, clinopyroxene and garnet system.

One interesting aspect of the Jabal Haylah websterite xenoliths is the uniqueness of their REE curves. The REE curves (Figure 4) for these samples are strange patterns because of the "dome" shapes, with the light and heavy REE being approximately equal and the middle REE are greater in abundance. Of the known accessory minerals that

concentrate REE, only apatite yields a similar "dome" pattern. However, the apatite pattern is more broader and generally has an associated negative anomaly (Nakasawa et al., 1969). No significant Eu anomaly was observed in these JH xenoliths. For these reasons, apatite may be ruled not as the REE carrier. These xenoliths are somewhat intermediate in composition between the basalts and the lherzolite type of rock. The samples have a much higher total REE content than the JT xenoliths. It seems possible that their unique REE patterns are dominated by the REE patterns in clinopyroxenes and that these xenoliths are also residue from a partial melting process.

Figure 10 is of special interest in that it shows how the two series of xenoliths fit into the chemical scheme developed by Kuno (1969). In this figure the $MgO/\Sigma FeO$ is plotted against the percent of the oxide of the elements. The average of the JT and JH samples fit into the diagram as expected with the exception of the Cr_2O_3 content of the JT samples. These extremely high Cr_2O_3 content could be due to the inclusion of chromium spinels. The $MgO/\Sigma FeO$ ratio is 2.3 for the average of the JH xenoliths and 6.3 for the average of the JT xenoliths.

The xenolith samples of this study show very strong agreement with other xenoliths that have been suggested as mantle material by other investigators in this field. The exact nature of how these rock samples originated is still under much debate and argument.

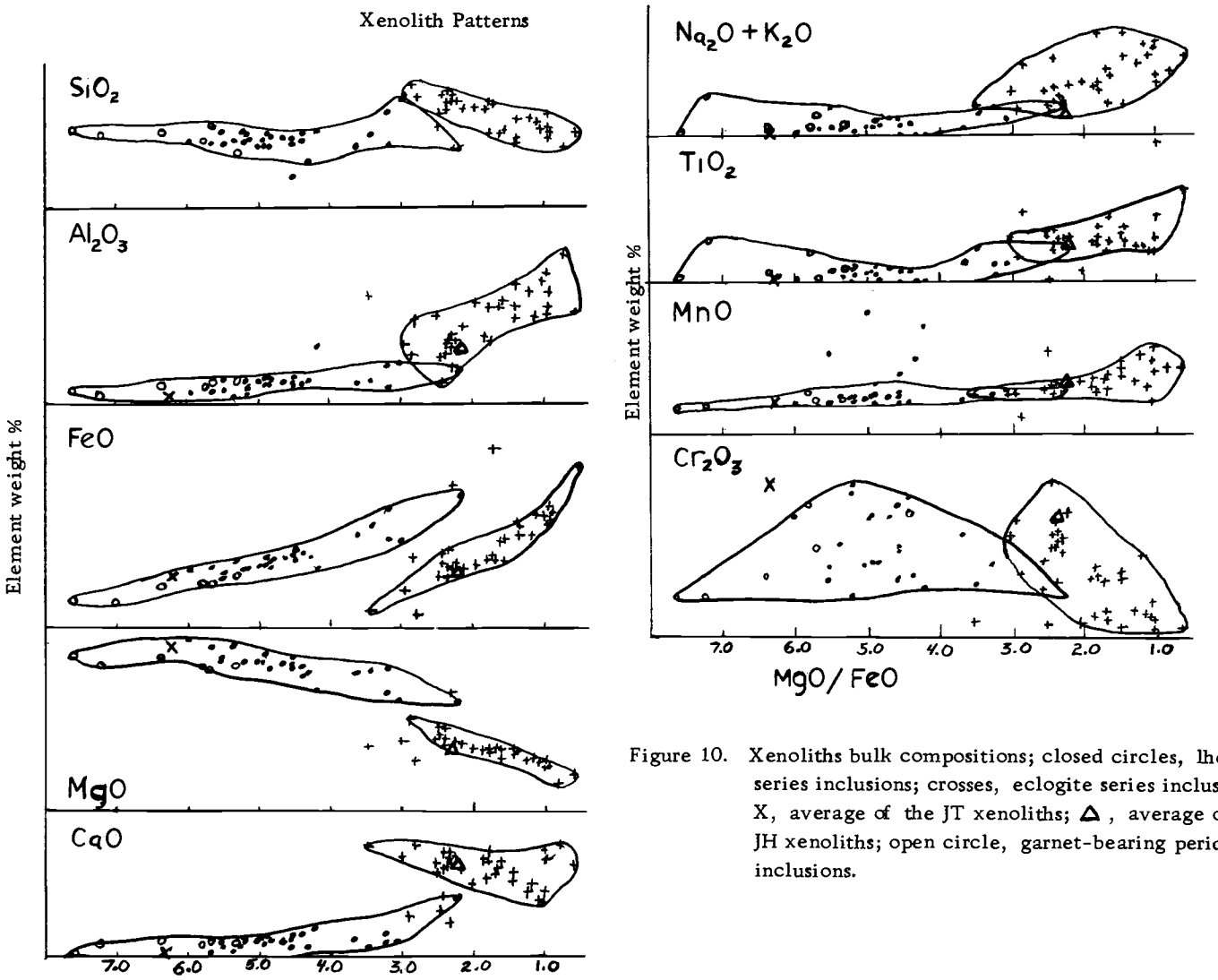

Figure 10. Xenoliths bulk compositions; closed circles, lherzolite series inclusions; crosses, eclogite series inclusions; X, average of the JT xenoliths; Δ, average of the JH xenoliths; open circle, garnet-bearing peridotite inclusions.

Mineral Partition Coefficients

The partition coefficients determined in this study are different from those determined previously because they are measured relative to the gabbro matrix. The bulk of the previous work was done relative to alkali basalts or to the theoretical liquid of the system. Attempts were made to determine the partition coefficients relative to the midoceanic ridge basalts but the values here showed no real pattern that would compare. The partition coefficients for the pyroxenes are relative to the mantle xenoliths discussed in the previous section. These can not be compared to the previous works of other investigators.

Ten of the plagioclase separates were used for the determination of partition coefficients. Six samples were from the Jabal Shayi series and four were from the Jabal at Turf series. The final average for the two series and also those of the pyroxene samples are shown in Table 8. The partition coefficients are somewhat larger than those found for the plagioclase-alkali basalts systems. The Eu anomaly, Eu/Eu* (where Eu is total chondritic normalized Eu and Eu* is the extrapolated value obtained from the average of the chondritic normalized Sm and Gd values), for the basalts is usually about 4, but the corresponding value for average plagioclase is about 10 in this study. The JT plagioclase series has partition values close

to those of the plagioclase in basalts but also shows a much greater Eu difference.

Table 8. Partition coefficients.

	JT Xenoliths		JH Xenolith	JS Gabbro	JT Gabbro
	O794 Opx	C793 Cpx	C797 Cpx	Average Plagioclase	Average Plagioclase
K	--	--	19	---	0.56
Rb	--	--	27	---	0.14
Cs	--	--	13	---	0.10
Sr	--	--	0.68	---	25
Ba	--	--	--	---	8.8
La	0.23	3.5	3.1	0.43 - 1.3	0.80
Ce	--	--	--	0.28 - 1.5	0.49
Sm	0.75	13	0.66	0.16 - 0.74	0.26
Eu	0.55	8.3	0.74	5.8 - 12.2	1.21
Tb	1.6	14.7	0.85	0.16 - 0.66	0.19
Yb	1.6	10.3	2.7	0.20 - 1.30	0.16
Lu	1.8	14.2	1.8	0.22 - 1.20	0.11
Th	--	--	--	0.14	0.33
Hf	0.24	2.9	0.80	0.04 - 0.15	0.062
Ta	0.1	--	0.2	310 - 860	82
Sc	2.4	8.5	0.72	0.01 - 0.03	0.009
Cr	1.6	2.0	4.0	0.001 - 0.03	0.004
Fe	0.78	0.45	0.50	0.04 - 0.09	0.074
Co	0.52	0.23	0.61	0.01 - 0.08	0.054

Basalts

The basalts analyzed in this work are from two distinct systems: three samples are from the Saudi Arabia area that are similar and six pairs of samples from the Columbia River basalts. The Sirat Plateau (SP) basalts are all similar in their bulk and minor element contents as well as their REE patterns. They all have high contents of Al_2O_3, MgO, Cr_2O_3 and the REE, and low contents of other trace elements, Sc, Co, etc relative to the gabbros. The REE curves again may resemble a mixture of continental and oceanic (tholeiitic) basalts. The SP basalts agree in most parts with those obtained by Coles (1972), differing only in their trace element contents. The only difference in the major element content is the higher (4-5% more) Al_2O_3 content of SAB 493. The remaining differences were in the trace elements of Cr_2O_3, Ba, Ta, Cs and V. The Ta content was higher in all of the samples analyzed as compared to those of Coles (1972). The Cs values were much lower and the V content was on the lower end of the range when compared to Coles' values. The Cr_2O_3 content of SAB 494 and the Ba content of SAB 493 are lower than the range cited by Coles (1972). The REE values and patterns are very similar to those SP basalts analyzed previously.

The Columbia River (Picture Gorge) basalts were not analyzed for their major or minor elements but mainly for their REE patterns.

The REE patterns of these samples are similar to those observed in SP basalts; however higher heavy REE abundances and a slight positive Eu anomaly were observed in some of these samples.

Rhyolite

The rhyolite sample is a volcanic ash sample that falls between the chemical composition of BCR-1 and GSP-1. It is low in FeO and CaO as is BCR-1, and is also high in Na_2O, Ba and the REE as is GSP-1. The REE pattern for the rhyolite sample is similar to the Sirat Plateau basalts, but shows a negative Eu anomaly.

A comparison with a paper by R. Coleman et al. (1973) is given in Appendix I since this paper was received after this study was completed and written.

V. CONCLUSION

Layered gabbros that intruded the Precambrian crust are thought to result from deep fracturing or foundering of the crust after the deformation of the mobile belts of rock that contained the magma. The wide spread occurrence of grabbroic intrusions suggests possible shallow melting within the upper mantle or lower crust. The origin of the layered gabbro series in the Red Sea area seem to be directly related to the structural development of the area. The Jabal at Turf layered series occupies a zone parallel to the dominant Red Sea. The Jabal Shayi layered series shows a similar chemical composition to the Jabal at Turf series and may be a central dome shaped finger of the magma (Coleman et al., 1972).

The Saudi Arabian gabbros may all be from the same or a very similar magma. This can be inferred because all the gabbro samples show similar REE patterns in both shape and content. The REE contents of these gabbros are below the Skaergaard Intrusion REE contents and also below the average oceanic tholeiitic content. The Saudi Arabian gabbros are considerably fractionated with respect to the midoceanic tholeiitic basalts.

The Jabal Shayi samples show no characteristic differences among samples by means of the major and minor element contents or by the REE patterns. The Jabal at Turf show some characteristic

differences in the samples. The major differences that are noted in the JT samples are found in the normalized REE patterns. In Figure 2 SAB 215, the possible chillzone sample has much higher REE content and a smooth pattern with no Eu anomaly. Gabbro SAB 491 has a much lower REE content than the other three layered gabbros. The lower REE content of SAB 491 may be explained by the high plagioclase content or the possibility of increased amount of trapped liquids in the other gabbroic rocks. The REE pattern from SAB 215 may be due to a partial melting of some lower crustal rock that is rich in Ca-minerals.

The xenoliths present some unexpected data. The xenoliths are from two distinct rock types discussed by Kuno (1969). Kuno plots the $MgO/\Sigma FeO$ against the major elements and this plot (Figure 10) clearly defines the two types as eclogites for the Jabal Halyah websterite xenoliths and lherzolites as the JT xenoliths. The JH xenoliths have interesting REE curves in that they are "dome" shaped and have greater total REE content than the JT samples. Both sets of xenoliths show extremely high (~1%) Cr_2O_3 values which is probably due to the inclusion of chromium spinels.

The elemental abundances of the mineral separates agree well with those obtained in other studies. These separates enable us to discuss the possible contribution of each mineral to the whole rock samples. This is seen in the REE patterns where the Eu anomaly

found in the whole rock is due to the plagioclase contribution. The contribution of the clinopyroxene to the Th content is also noted.

The basalts studied for this work are all similar in the REE patterns even though the samples are from two different systems, SAB samples and Picture Gorge samples. The major and minor elemental contents for the SAB samples agree well with those determined by Coles previously.

BIBLIOGRAPHY

Boynton, W. V. 1973. Oregon State University. Personal communication. Corvallis, Oregon.

Brown, G. F. 1970. Eastern Margin of the Red Sea and the Coastal Structures in Saudi Arabia. Philosophical Transactions of the Royal Society of London. Vol. 267. pp 75-87. London.

Clarke, Franke W. 1924. The Data of Geochemistry. Washington Government Printing Office.

Coleman, Robert G. 1972-1973. Branch of Field Geochemistry and Petrology, United States Geological Survey. Personal Communications with R. A. Schmitt and D. A. Miller. Menlo Park, California.

Coleman, R. G. 1972. Geologic Background of the Red Sea. U.S. Geological Survey. Preprint.

Coleman, R. G.; Brown, G. F. and Keith, T. E. C. 1972. Layered Gabbros in Southwest Saudi Arabia. U.S. Geological Survey Research Prof. Paper 800-D. pp D143-D150.

Coleman, R. G.; Fleck, R.; Hedge, C. E. and Ghent, E. D. 1973. The Volcanic Rocks of Southwestern Saudi Arabia and the Opening of the Red Sea. U. S. Geological Survey. Preprint.

Coles, David G. 1972. Chemical Compositional Studies of Marginal Rift and Plateau Basalts from Saudi Arabia. M.S. Thesis. Oregon State University. Corvallis, Oregon.

Curtis, David B. 1973. Oregon State University. Personal Communication. Corvallis, Oregon.

Filby, R. H.; Davis, A.; Shah, K.; Wainscott, G.; Haller, W.; and Gasatt, W. 1970. Gamma Ray Energy Tables for Neutron Activation Analysis. Washington State University Press. Pullman, Washington.

Flanagan, F. J. 1972. 1972 Values for International Geochemical Reference Samples. Geochimica et Cosmochimica Acta. Vol. 37. Pergamon Press Ltd. London. pp 1189-1200.

Frey, Fred A. 1969. Rare Earth Abundances in a High-Temperature Peridotite Intrusion. Geochimica et Cosmochimica Acta. Vol. 33. Pergamon Press Ltd. London. pp 1429-1447.

Goldschmidt, V. M. 1958. Geochemistry. Oxford University Press. London.

Goles, Gordon G. 1973. Professor. University of Oregon. Personal Communications. Eugene, Oregon.

Gordon, Glen E.; Randle, Keith; Goles, Gordon G.; Corliss, John B.; Beeson, Marvin H.; and Oxley, Susanna S. 1968. Instrumental Activation Analysis of Standard Rocks with High-Resolution γ-Ray Detector. Geochimica et Cosmochimica Acta. Vol. 32. Pergamon Press Ltd. London. pp 369-396.

Green, D. H. and Ringwood, A. E. 1967. An Experimental Investigation of the Gabbro to Eclogite Transformation and its Petrological Applications. Geochimica et Cosmochimica Acta. Vol. 31. Pergamon Press Ltd. North Ireland. pp 767-833.

Green, D. H. and Ringwood, A. E. 1969. The Origin of Basalt Magmas. The Earth's Crust and Upper Mantle. Pembroke J. Hart, Editor. Geophysical Monograph 13. American Geophysical Union. Washington D. C. pp 489-495.

Hamilton, E. 1959. The Uranium Content of the Differentiated Skaergaard Intrusion. Meddelelser om Gronland. Bd. 162. Nr. 7. C. A. Reitzels Rorlag - Kobenhavn.

Harris, P. G.; Reay, A.; and White, I. G. 1967. Chemical Composition of the Upper Mantle. Journal of Geophysical Research. Vol. 72. No. 24. pp 6359-6369.

Haskins, L. A. and Frey, F. A. 1966. Dispersed and Not-So-Rare Earths. Science. Vol. 152. No. 3720. pp 299-314.

Haskins, L. A. and Haskins, M. A. 1968. Rare-Earth Elements in the Skaergaard Intrusion. Geochimica et Cosmochimica Acta. Vol. 32. No. 4. Pergamon Press Ltd. London. pp 433-448.

Helmke, Philip A. and Haskin, Larry A. 1972. Rare-Earth Elements. Co, Sc, and Hf in the Steens Mountain Basalts. Preprint.

Hess, H.H. and Poldervaart, Arie. 1967. Basalts: The Poldervaart Treatise on Rocks of Basaltic Composition. Vol. 1. Interscience Publishers. John Wiley and Sons. New York - London - Sydney.

Jensen, Brenda B. 1973. Patterns of Trace Element Fractionation. Preprint.

Kay, R.; Hubbard, N.J. and Gast, P.W. 1970. Chemical Characteristics and Origin of Oceanic Ridge Volcanic Rocks. Journal of Geophysical Research. Vol. 75. American Geophysical Union. pp 1585-1613.

Kay, Robert and Senechal, R.G. 1973. The Troodos Ophiolite is a Piece of Mesozoic Ocean Floor: Rare Earth Evidence. Preprint.

Kuno, Hisashi. 1969. Mafic and Ultramafic Inclusions in Basaltic Rocks and the Nature of the Upper Mantle. The Earth's Crust and Upper Mantle. P.J. Hart, Editor. Geophysical Monograph 13. American Geophysical Union. Washington D.C. pp 507-513.

Laul, J.C. 1973. Oregon State University. Personal Communication. Corvallis, Oregon.

Laul, J.C. and Schmitt, R.A. 1973. Chemical Composition of Apollo 15, 16 and 17 Samples. Preprint.

Laul, J.C. and Schmitt, R.A. 1972. Bulk and REE Abundances in Three Apollo 15 Igneous Rocks and Six Basaltic Rake Samples. The Apollo 15 Samples. J.W. Chamberlain and C. Watkins, Editors. Lunar Science Institute, Houston. pp 225-228.

Lowell, James D. and Genik, Gerard J. 1972. Sea-Floor Spreading and Structural Evolution of Southern Red Sea. The American Association of Petroleum Geologists Bulletin. Vol. 56. The American Association of Petroleum Geologists. pp 247-259.

Mason, Brian. 1965. Principles of Geochemistry. Second Edition. John Wiley and Sons, Inc. London.

Megrue, G.H.; Norton, E. and Strangway, D.W. 1972. Tectonic History of the Ethiopian Rift as Deduced by K-Ar Ages and Paleomagnetic Measurements of Basaltic Dikes. Journal of Geophysical Research. Vol. 77. American Geophysical Union. pp 5744-5754.

Montigny, R.; Bougault, H.; Bottinga, Y. and Allegre, C.J. 1973. Trace Element Geochemistry and Genesis of the Pindos Ophiolite Suite. Geochimica et Cosmochimica Acta. Vol. 37. Pergamon Press Ltd. London. pp 2135-2147.

Nagasawa, H.; Wakita, H.; Hiquchi, H. and Onuma, N. 1969. Rare Earths in Peridotite Nodules: An Explanation of the Genetic Relationship between Basalt and Peridotite Nodules. Earth and Planetary Science Letters. Vol. 5. North-Holland Publishing Co. Amsterdam. pp 377-381.

Norman, J.C. and Haskin, L.A. 1967. The Geochemistry of Sc: A Comparison to the Rare Earths and Fe. Geochimica et Cosmochimica Acta. Vol. 32. Pergamon Press Ltd. London. pp 93-108.

Oertel, A.C. 1969. Frequency Distribution of Element Concentrations - I. Theoretical Aspects. Geochimica et Cosmochimica Acta. Vol. 33. Pergamon Press Ltd. London. pp 821-831.

Oertel, A.C. 1969. Frequency Distribution of Element Concentrations - II. Surface Soils and Ferromagnesian Minerals. Geochimica et Cosmochimica Acta. Vol. 33. Pergamon Press Ltd. London. pp 833-839.

Osawa, Masumi and Goles, Gordon G. 1972. Trace Element Abundances in Columbia River Basalts. Proceedings of the Second Columbia River Basalt Symposium. pp 55-71.

Paster, T.P.; Schauweckert, D.S.; and Haskins, L.A. 1973. The Behavior of Some Trace Elements During Solidification of the Skaergaard Layered Series. Preprint.

Philpotts, J.A. and Schnetzler, C.C. 1970. Phenocryst-matrix partition coefficients for K, Rb, Sr, and Ba, with Applications to Anorthosite and Basalt Genesis. Geochimica et Cosmochimica Acta. Vol. 34. No. 3. Pergamon Press Ltd. London. pp 307-322.

Rankama, K. and Sahama, G. 1950. Geochemistry. University of Chicago Press. Chicago.

Ringwood, A.E. 1972. The Chemical Composition and Origin of the Earth. Preprint Chapter. pp 287-356.

Schilling, J.G. 1971. Sea-Floor Evolution: Rare-Earth Evidence. Philosophical Transactions of the Royal Society of London. Vol. 268. London. pp 663-706.

Schilling, J.G. 1973. Afar Mantle Plume: Rare Earth Evidence. Nature. Vol. 242. MacMillan Journals Ltd. London. pp 2-5.

Schmitt, R.A. 1973. Professor. Oregon State University. Personal Communication. Corvallis, Oregon.

Schmitt, R.A.; Linn, T.A. and Wakita, H. 1970. The Determination of Fourteen Common Elements in Rocks via Sequential Instrumental Activation Analysis. Radiochimica Acta. Vol. 13. pp 200-212.

Schnetzler, C.C. and Philpotts, J.A. 1968. Partition Coefficients of Rare Earth Elements and Barium between Igneous Matrix Material and Rock-Forming Mineral Phenocrysts - I. Origin and Distribution of the Elements. L.H. Ahrens, Editor. Pergamon Press Ltd. London. pp 929-938.

Schnetzler, C.C. and Philpotts, J.A. 1970. Partition Coefficients of Rare-Earth Elements between Igneous Matrix Material and Rock-Forming Mineral Phenocrysts - II. Geochimica et Cosmochimica Acta. Vol. 34. No. 3. Pergamon Press Ltd. London. pp 331-340.

Shaw, D.W. 1961. Element Distribution Laws in Geochemistry. Geochimica et Cosmochimica Acta. Vol. 23. Pergamon Press Ltd. London. pp 116-134.

Stueber, Alan M. and Goles, Gordon G. 1967. Abundances of Na, Mn, Cr, Sc, and Co in Ultramafic Rocks. Geochimica et Cosmochimica Acta. Vol. 31. Pergamon Press Ltd. London. pp 75-93.

Wager, L.R. and Mitchell, R.L. 1951. The Distribution of Trace Elements During Strong Fractionation of Basic Magma - A Further Study of the Skaergaard Intrusion, East Greenland. Geochimica et Cosmochimica Acta. Vol. 1. No. 3. Pergamon Press Ltd. London. pp 129-208.

Wager, L.R. and Brown, G.M. 1967. Layered Igneous Rocks. W.H. Freeman and Co. San Francisco, Cal.

Wheeler, Robert R. 1970. Oil in the Red Sea: Rift or Drift. World Oil. pp 53-57.

Whittaker, E.J.W. 1967. Factors Affecting Element Ratios in the Crystallization of Minerals. Geochimica et Cosmochimica Acta. Vol. 31. Pergamon Press Ltd. London. pp 2278-2288.

Whittaker, E.J.W. and Muntus, R. 1970. Ionic Radii for Use in Geochemistry. Geochimica et Cosmochimica Acta. Vol. 34. Pergamon Press Ltd. London. pp 945-956.

APPENDIX

APPENDIX I

The values obtained in this work agree well with those published by Coleman et al. (1973). The values by Coleman were on splits of the identical samples that were analyzed for this study. The values for the major elements agree well except for a slightly lower concentration of the alkali oxides than determined by Coleman et al. The minor elements agree well except for the V content which Coleman et al. found much higher.

Coleman et al. also suggests that the layered gabbros could chemically be derived from the chillzone material (SAB 215) by fractional crystallization. They stated that the JT dike swarms may represent the residual liquid from the JT layered gabbro intrusion. In comparing the normalized REE pattern in dike samples, determined by Coles (1972), with that of the chillzone material, it is noted that the total REE content is enriched in the dike samples as it should be in a residual liquid. One problem encountered here is that there is no negative Eu anomaly as would be expected after the removal of the plagioclase in the gabbros. All of the gabbros analyzed show a positive Eu anomaly and removing this from the chillzone like magma should give some degree of negative Eu anomaly.

Coleman et al. (1973) find no variation among the layered gabbros due to the layering or the height factor as was found in this

study. Through chemical analysis it appears that this JT gabbro system was not formed in a manner similar to the Skaergaard Intrusion of Eastern Greenland.